Non-Gaussian Noise in Superconducting Circuits

by

Trevor Johnathan McCourt

B.ASc Mechanical Engineering, University of Waterloo (2020)

Submitted to the Department of Electrical Engineering and Computer Science
in partial fulfillment of the requirements for the degree of

MASTER OF SCIENCE

at the

MASSACHUSETTS INSTITUTE OF TECHNOLOGY

September 2023

Authored by:	Trevor Johnathan McCourt Department of Electrical Engineering and Computer Science August 16, 2023
Certified by:	Isaac L. Chuang Professor of Electrical Engineering and Computer Science Thesis Supervisor
Accepted by:	Leslie A. Kolodziejski Professor of Electrical Engineering and Computer Science Chair, Department Committee on Graduate Students

Non-Gaussian Noise in Superconducting Circuits

by

Trevor Johnathan McCourt

Submitted to the Department of Electrical Engineering and Computer Science
on August 20, 2023, in partial fulfillment of the
requirements for the degree of
Master of Science

Abstract

In stark contrast to man-made systems, living things embrace noise and use it to further their functionality. It is therefore not surprising that some lifeforms couple strongly to environmental fluctuations, and can leverage non-Gaussian noise to gain a competitive edge over their peers. In this thesis, I study non-Gaussian fluctuations using a system of Transmon qubits as ultra-sensitive quantum sensors and make the first clear experimental observation of non-Gaussian noise in a qubit system. I achieve this using multi-qubit dynamical decoupling sequences that characterize noise during two-qubit gates when the system is coupled strongly to flux fluctuations. This noise is qualitatively different from the well-studied noise that leads to single qubit dephasing; it simultaneously affects the two qubits, inducing fluctuations in their entangling parameter. In our superconducting system, the experimentally observed noise is consistent with random telegraph noise and leads to the stepwise decay of signals. With this clear characterization of non-Gaussian noise in hand, we have paved the way for a new class of lifelike engineered systems that harness noise to their benefit.

Thesis Supervisor: Isaac L. Chuang
Title: Professor

Acknowledgments

Thanks to Vadim, Andre, and Charles for taking an unreasonable amount of time to teach this stubborn engineer how to be a physicist. Thanks to Ike for being the ideal PhD advisor, and always pushing me to ask nature bigger and better questions. Onwards and upwards!

Contents

List of Figures

Chapter 1

Introduction

One of the most compelling features of the physical world is how random it appears to be. Even though the vast majority of phenomena that we observe day-to-day are described by a deterministic set of physical laws, many of them still seem to be unpredictable. The fundamental reason for this is that any finite agent, such as ourselves, can only ever keep track of the state of a finite number of environmental degrees of freedom. Therefore, over time, it is inevitable that an agent will lose track of parts of its environment, and will only be able to reason about it in probabilistic terms. Noise, it seems, is a fundamental feature of the environments occupied by living things.

In the world of engineering, noise is almost always considered to be detrimental, as it refutes our efforts to build perfectly predictable and reliable devices. We have gone to great lengths to develop techniques to minimize the effect of noise on engineered systems. The study of such techniques birthed the field of error correction [1], which studies the limits of the transmission of information through noisy channels. In stark contrast to this, for living things, noise is not at all purely detrimental. Noise endows living things with the ability to explore their environment, granting them abilities and resources that would be inaccessible if they followed entirely deterministic trajectories. Noise is fundamental to the function of living things.

Further, in this work, we will argue that living things are able to gain a competitive advantage in exploratory ability by coupling strongly to sources of noise, such that

the statistics of the noise are not Gaussian. This non-Gaussian noise is strongly atypical in engineered systems, and therefore has not been microscopically explored to date. Towards leveraging this non-Gaussian noise in physical devices, we devise and implement a protocol for measuring and characterizing non-Gaussian noise in a system of quantum bits (qubits).

In section 1.1, we provide some examples of how living things use noise to explore their environments, and then in section 1.2 we outline the standard physical model of diffusion, which is how exploration is usually modeled in physics. In section 1.3, we provide several examples of living things using non-Gaussian noise to explore faster, in violation of the previously described physical models. In sections 1.4, 1.5, and 1.6 we go on to justify and outline an experimental protocol for characterizing such non-Gaussian fluctuations in a microscopic physical system for the first time, towards harnessing it to allow engineered devices to explore as if they were alive.

1.1 Noise and Life

The role of noise in driving exploration in living things is evident at many scales and levels of abstraction.

At the lowest level, evolution, the process by which all known living things have emerged, is heavily reliant on noise. Genetic mutations, caused by random environmental fluctuations, are the fundamental driver of generational change (and sometimes improvement) in populations of organisms [2, 3]. Noise in evolution drives exploration in the space of possible living things.

More concretely, genetic circuits, which regulate cell functionality, have long been known to be noisy. This noise was originally assumed to be detrimental, but recently it has begun to be understood as crucial to cell functionality [4]. Noise causes cells to express different genes at different times. This allows them to implement strategies like dividing labor between cells of different specializations that are difficult to achieve deterministically [5]. This stochasticity in gene expression leads to complex and beneficial behavior at the multi-cellular level. For example, bacteria have evolved to

quasi-randomly switch between states of vulnerable growth and protected persistent states, in which they do not grow but are better defended against antibiotics [6]. This persistent state allows populations of bacteria to survive antibiotic treatments, at the cost of stunted growth. Noise drives exploration of the space of possible functionalities of an organism, and helps keep them alive.

Small organisms such as bacteria routinely harness noise to move through space. The ability of bacteria to control their motion varies from species to species. Some can only move in a single direction and therefore are entirely reliant on environmental fluctuations to move in anything other than a straight line [7]. More advanced species are equipped with orientation control, and yet they still seem to move randomly. For example, E-coli move via the famous "run and tumble" procedure [8], in which an organism moves by repeating straight-line motion at a constant speed followed by a seemingly random change in direction. Bacteria make up most of the earth's biomass [9], so it is reasonable to state that noise is largely responsible for the ability of living things to physically explore their environment.

Noise is also critical to the ability of higher organisms to learn. There are two fundamentally opposed ways for an organism to act successfully in an environment. It can exploit what it already knows, and act in a way that is optimal according to its internal model. Exploitation can in principle be entirely deterministic. Alternatively, an organism can choose to explore its environment, expanding its knowledge. Since exploration implies moving into areas where knowledge is incomplete, it is an inherently stochastic process and must rely on noise in some fashion. Optimal outcomes are achieved by balancing exploration and exploitation, known as the "explore exploit tradeoff" [10]. Noise is essential to the ability of higher organisms to learn and acquire new abilities.

1.2 Brownian motion and thermal noise

Statistical physics is dedicated to the study of the physical implications of this ever-present noise. Foundational in statistical physics is Brownian motion. Discovered

by Einstien [11], Brownian motion occurs when a few observable degrees of freedom weakly interact with a large bath of unobserved degrees of freedom. This kind of system is realizable in many different physical substrates, such as particles suspended in fluids [12] and electric circuits [13]. For a Hamiltonian system, Brownian motion is modeled using the Langevin equation, given in dimensionless and integral form as,

$$\begin{aligned} dx =& p\, dt \\ dp =& \left(-\frac{dV(x)}{dx} - p \right) dt + \sqrt{2}\, dW_t \end{aligned} \tag{1.1}$$

This is the Langevin equation for a single particle; it is easily generalized to larger systems. Here x and p are dimensionless effective position and momentum variables, and $V(x)$ is a dimensionless effective potential. x, p, t, and V are related to the true Hamiltonian coordinates, time, and potential of the system of interest by scale factors. In particular, $V = \frac{E}{k_B T}$, where E is the potential energy of the system of interest, and $t = \gamma\tau$, where τ is the original time coordinate and γ is a friction coefficient. dW_t is the incriment of a Weiner process.

The essence of the exploratory nature of Brownian motion may be understood by solving the Langevin equation for a free particle, $V = 0$. Of particular interest is the variance of position over time, as this describes how far a particle will drift from its initial state as a function of time. Using the methods of Ito calculus, we can easily find that,

$$\left\langle \left(x(t) - \langle x(t) \rangle \right)^2 \right\rangle = e^{-2t} \left(4e^t - 1 \right) + 2t - 3 \tag{1.2}$$

for $t \ll 1$,

$$\sqrt{\left\langle \left(x(t) - \langle x(t) \rangle \right)^2 \right\rangle} \approxeq \sqrt{\frac{2}{3}} t^{3/2} \tag{1.3}$$

and for $t \gg 1$,

$$\sqrt{\left\langle \left(x(t) - \langle x(t) \rangle \right)^2 \right\rangle} \approxeq \sqrt{2t} \tag{1.4}$$

So at long times, on average, the particle explores away from the origin a distance that grows with $\sqrt{t}$. At short times, exploration is slow, growing as $t^{3/2}$.

One of the main experimental observations the Langevin equation was designed

to reproduce was the convergence to Boltzmann statistics at large times,

$$p(x, p, t \to \infty) = \frac{1}{Z} e^{-\frac{p^2}{2}} e^{-V(x)} \tag{1.5}$$

where $p(x, p, t)$ is the probability density corresponding to the state (x, p) at time t, and Z is a partition function that ensures the distribution is normalized. Physically, this convergence requires that the interaction of the system with the bath be weak, and also that the bath have a short memory, which can be achieved by forming the bath out of a very large number of degrees of freedom. Via appeal to the central limit theorem, it is therefore intuitive that the Weiner process, a Gaussian process that is uncorrelated in time, shows up in 1.2.

Generally, a random process $X(t)$ is considered Gaussian if the joint distribution of $\{X(t_1), \ldots, X(t_N)\}$ for an arbitrary set of t_j is Gaussian. An equivalent condition that is often useful is that for any g(t) satisfying,

$$\int_0^t |g(\tau)| d\tau < \infty \tag{1.6}$$

the following produces a random variable $Y(t)$ that has a Gaussian distribution,

$$Y(t) = \int_0^t g(\tau) X(\tau) d\tau \tag{1.7}$$

1.3 Non-Gaussian noise and life

Historically, the Langevin equation and other Gaussian models that incorporate memory [14, 15] have been widely successful in accounting for fluctuation and dissipation in physics experiments. This is likely because experiments are intentionally designed to be precise, and couple to thermal noise as weakly as possible. However, there is no reason a-priori for this to be the case for living things. Since noise can be beneficial to the functionality of living things, evolution may have pushed living things to couple more strongly to a smaller number of noise sources. The central limit theorem will not apply in this case, and the noise may very well be non-Gaussian.

For example, consider the previously mentioned run-and-tumble motion of E-coli. Experimental observations of this motion reveal that it is composed of periods of straight-line motion interrupted by random relative directional changes. The time between directional changes is well modeled by an exponential distribution [16], and directional changes correspond to a rotation of the direction of travel by the nearly constant angle $\pm\varphi$. Therefore, a trajectory corresponds to repeatedly moving at a constant speed until a random direction change event occurs, and then applying a rotation sampled from a sharp bimodal distribution, with maxima at $\pm\varphi$. The noise involved in this process is non-Gaussian. Following the analysis of [17], the variance in displacement $d = |r(t) - r(0)|$ as a function of time is given by,

$$\langle (d(t) - \langle d(t) \rangle)^2 \rangle = 2D \left(t - 1 + e^{-t} \right) \tag{1.8}$$

where D is the diffusion constant and t is the appropriate dimensionless time. Working in units where $D = 1$ and taking the short time limit $t \ll 1$,

$$\sqrt{\langle (d(t) - \langle d(t) \rangle)^2 \rangle} \propto t \tag{1.9}$$

and for $t \gg 1$,

$$\sqrt{\langle (d(t) - \langle d(t) \rangle)^2 \rangle} \propto \sqrt{2t} \tag{1.10}$$

Comparing 1.4 and 1.10, it is clear that at long times the rate of exploration for Brownian motion and this non-Gaussian motion is the same, however at short times the non-Gaussian process has a smaller power and therefore grows faster, see Fig. 1-1. Therefore, this particular non-Gaussian fluctuation provides an initial exploratory advantage to organisms that can couple to it.

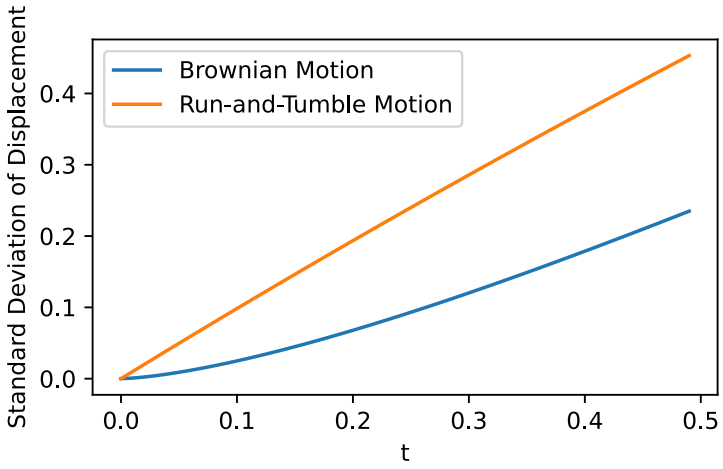

Figure 1-1: **Comparing the short-time behavior of run-and-tumble and Brownian motion** Exploration is linear at short times for run-and-tumble motion, and less than linear for Brownian motion.

Another example of living systems gaining an advantage by coupling to non-Gaussian noise is found in the study of active matter. Active matter consists of large systems of self-propelled particles undergoing noisy dynamics. The effective noise that drives the system is both non-white and non-Gaussian [18]. One of the interesting things that happens in active matter systems is that they exhibit large-scale flocking behavior even when the forces between the particles are strictly repulsive. This behavior deviates strongly from what would be expected at thermal equilibrium for Langevin dynamics, which would predict a nearly uniform distribution of the particles. By considering a modified set of equations where the noise is white but non-Gaussian, it has been shown that the non-Gaussianity rather than the memory in the noise is the main driver of this flocking behavior [19]. Therefore, it seems that coupling to non-Gaussian noise can drive primitive social behavior in living things.

A third example of the advantages of non-Gaussian noise can be found in the escape from metastable states. Here, a particle moves from one potential minimum to another via the action of noise, in the process surmounting a potential energy barrier of height ΔE. In the case of Langevin dynamics, it is well understood that

the rate of hopping between the two wells scales as $e^{\frac{\Delta E}{k_B T}}$ [20]. It has been found that for non-Gaussian noise of the same power, the rate of transitions is strictly faster than in the Gaussian case. In particular, the transition rate is e^S, where $S < \frac{\Delta E}{k_B T}$ [21]. As such, non-Gaussian noise provides an exponential advantage in hopping between metastable states. Non-Gaussian noise provides a strong advantage in the rapid exploration of rugged potential landscapes.

1.4 Measuring non-Gaussian noise using quantum systems

From all of these examples, it is clear that living things routinely harness non-Gaussian noise to further their own exploratory capabilities. As previously mentioned, this is quite different to how engineered systems function, which generally couple weakly to noise and behave as deterministically as possible. Is this really the best way forward? Can we design systems that couple strongly to non-Gaussian noise that can explore as effectively as living things?

One difficulty with this proposition is that realizing non-Gaussian noise in macroscopic systems is difficult. The fundamental reason for this is the central limit theorem, which states that the sum of a large number of independent random variables is Gaussian, regardless of the distributions of the variables in isolation. Engineered systems tend to be large, and therefore they couple to many noisy degrees of freedom, which result in an effective Gaussian noise. This is the basic reason for the ubiquity of Gaussian noise in engineered devices.

Engineered quantum devices may be an exception to this rule. Quantum devices are inherently small, limiting their ability to couple to environmental degrees of freedom. They are also generally designed to be shielded from noise to improve quatnum coherence. Therefore, it seems feasible that an engineered quantum system may couple to only a few fluctuating degrees of freedom, operating outside the central limit theorem regime, allowing for a precice study of non-Gaussian noise. Indeed, quantum

systems have previously been found to be extremely sensitive to physical noise and form useful platforms for probing it [22]. Conveniently for those interested in studying noise, one of the major challenges associated with building a large-scale quantum computer is understanding and mitigating noise. Noise studies using qubits as ultra-sensitive sensors serve the dual purpose of increasing our understanding of noise in the physical world and helping us build better quantum computers.

With this in mind, in this thesis I ask if it is possible to unambiguously observe and characterize in detail non-Gaussian noise in a qubit system? This will involve both a substantial theoretical work and also experiments in a superconducting qubit system. Superconducting qubits are essentially non-linear electrical oscillators operating at energy levels comparable with $\hbar\omega$ [23]. In particular, we will study noise that affects two-qubit gates in a tunable coupler Transmon qubit system [24]. This kind of system has enjoyed a high degree of computational success in the areas of quantum simulation [25, 26, 27], quantum chemistry [28], and theoretical computer science [29, 30, 31, 32]. Imperative to this is the ability to generate entanglement using high-fidelity two-qubit gates [33, 34]. As control of these gates is improved, their performance will start to become limited by system-environment interaction. The characterization and eventual mitigation of this noise-producing interaction is therefore critical to continual forward progress.

1.5 Qubit noise characterization

Traditionally, the bulk of low-frequency noise characterization in qubits has been dedicated to the study of single-qubit dephasing noise. This is modeled as either a qubit coupling to external quantum degrees of freedom or as classical stochastic fluctuations in the qubit frequency [35]. Most often, the noise is assumed to have Gaussian statistics. In this Gaussian scenario, sophisticated tools have been developed to characterize the power spectral density of the noise [36, 37, 38, 39]. There have also been efforts to characterize noise outside of this regime. These have been focused on measuring the higher-order moments of single-qubit non-Gaussian dephasing [40, 41]

as well as characterizing spatially correlated Gaussian dephasing noise [42, 43, 44].

Studies of single-qubit dephasing may be sufficient to understand the behavior of small systems involving only one or a few qubits. However, large systems have many degrees of freedom, and therefore many channels through which noise can enter. For example, noise that occurs during two-qubit gates may lead to noise that affects two qubits simultaneously. Understanding these two-qubit noise mechanisms in the context of quantum computing will be important for implementing near-term quantum algorithms and building a fault-tolerant quantum computer in the long term. Indeed, recent work has begun to develop methods for characterizing multi-qubit noise [45, 46]. Experimentally, the difficulty in characterizing noise in larger systems stems from the fact that the measurement of a particular kind of noise may be confounded by competing error mechanisms, as larger systems are generally more difficult to control precisely than small ones.

1.6 Noisy two-qubit gates

In this work, we characterize noise that occurs during two-qubit gates. The gate we study is performed using a tunable coupler that modulates the qubit-qubit coupling. Our key observation is that the primary source of noise is the frequency fluctuations of this coupler. These fluctuations lead to noise in the entangling parameter g, the coupling strength between the two qubits. The noise is therefore turned on during a gate operation and affects two qubits simultaneously, in qualitative distinction from single-qubit dephasing. We show that this fundamentally two-qubit noise can be studied by driving pairs of qubits through two-qubit pulse sequences with interleaved coupler and qubit frequency control. We find that in many samples this noise is composed of Gaussian $1/f$ noise, similar to the noise dominating single qubit dephasing, and a signal from a few random telegraph fluctuators. These findings are significant because both the two-qubit and non-Gaussian nature of the observed noise may require new error mitigation techniques [47]. Additionally, the clean signatures of non-Gaussian noise that we see are a significant departure from what is typically

assumed and observed in condensed matter systems, where Gaussian $1/f$ noise is ubiquitous [48, 49, 50, 51].

At an intuitive level, the quantum system we characterize in this thesis may be understood via the mechanical system shown in figure 1-2.

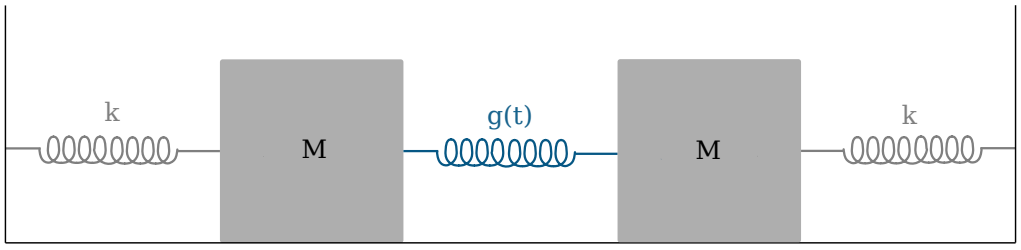

Figure 1-2: **An intuitive model for the Transmon-coupler-Transmon system** Each mass and spring models a Transmon qubit, and the blue spring with tunable rate represents the coupler.

Each mass (labeled M) is connected to a rigid wall via a spring with stiffness k. Each collective mass-spring system represents a Transmon qubit. The two masses are coupled by a spring that has controllable stiffness $g(t)$. This represents the tunable coupler. If $g = 0$, the masses are uncoupled, and their dynamics are completely independent. A nonzero g allows the masses to exert forces on one another.

A two-qubit gate may be understood in this system as transferring a precise amount of energy between the masses by modulating $g(t)$. This operation should be as fast as possible, as this allows the quantum computer to run faster. The operation also has to be accurate: the transfer of energy must be precise. Transferring too much or too little energy corresponds to an error in the gate operation.

If g could be perfectly controlled, this problem may be difficult, but entirely solvable. Unfortunately, things are not quite so simple in reality. As will be revealed in later chapters, in our system $g(t)$ is not deterministic and inevitably fluctuates due to experimental imperfections. To make matters worse, the noise in g gets stronger as g is increased. So as one tries to make a gate faster, it also becomes noisier. This represents a fundamental upper bound on gate performance. As such, we would like

to understand and characterize these fluctuations in our device.

One factor that confounds this characterization is that $g(t)$ is not a directly experimentally measurable quantity. In general, we can only measure things about the degrees of freedom of the two masses, for example, their positions. Therefore, to study fluctuations in g, we will have to devise a way to infer them indirectly from measurements of the two masses. Devising such an experiment and interpreting the results is the central focus of this thesis.

1.7 Overview of the thesis

In chapter 2, we will start by introducing an appropriate quantum-mechanical model for the Transmon-coupler-Transmon system and using it to gain a precise understanding of how noise in experimental control parameters manifest themselves as noise in g. Using this physical model, in chapter 3 we will then devise an experimental scheme for characterizing fluctuations in g. In chapters 4 and 5, we will derive detailed models that predict how Gaussian and non-Gaussian fluctuations will manifest themselves in our measurement protocol. Finally, in chapter 6, we will implement our measurement protocol on one of Google's tunable coupler Transmon devices and analyze the results.

This thesis elaborates on results presented in my Physical Review A paper [52]. The reader is encouraged to look there if they prefer a more concise presentation of these results.

Chapter 2

The Tunable Coupler Transmon

The investigations in this work are centered around a particular superconducting qubit architecture, the *tunable-coupler Transmon*. In this chapter, we will briefly overview the relevant physics of these devices, and develop our model for how noise in the coupler control parameter affects its operation. This chapter will not go into all the details of the physical derivations, as those were not the focus of this work and have little bearing on its results. The interested reader should consult with the references cited within. Specifically, in section 2.1 we will introduce the tunable coupler Transmon circuit and explain how magnetic flux is used to tune the circuit parameters. We will then present a quantum-mechanical Hamiltonian for the circuit in section 2.2, and show how fluctuations in this control flux lead to fluctuations in the parameters of this Hamiltonian in section 2.3.

2.1 Circuit Diagram and Flux Control

The Transmon qubit is a loop composed of a large capacitor and a non-linear inductance [24]. In the Tunable coupler Transmon architecture, two-qubit Transmons are connected via a 3rd Transmon, designated as the coupler [53]. This is shown schematically in Fig. 2-1.

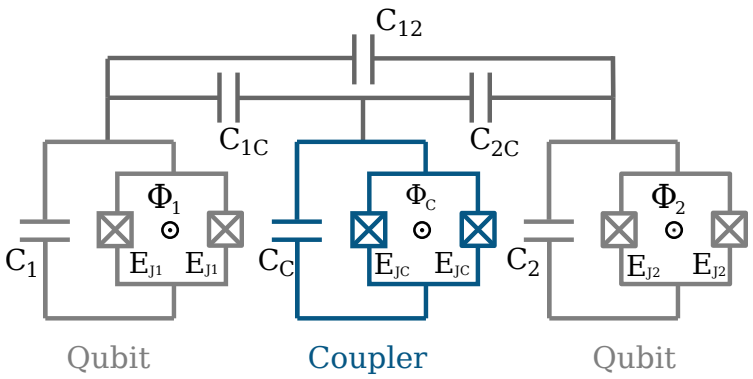

Figure 2-1: **Simple schematic of the tunable coupler transmon** Simplified circuit diagram for two qubits and the tunable coupler.

Typically, the non-linear inductance present in the qubits and coupler is made using two Josephson junctions in parallel threaded by an external flux, as indicated in the figure. Each junction has Josephson energy E_j and the external flux is indicated by Φ. This parallel combination is equivalent to a virtual junction with an effective flux-tunable Josephson energy,

$$E_j^{\text{eff}} = 2E_j \left| \cos\left(\frac{\pi\Phi}{\Phi_0}\right) \right| \tag{2.1}$$

where Φ_0 is the magnetic flux quantum. As such, we can see that the flux allows the inductance in each loop to be tuned, providing a control knob that allows one to alter the configuration of the circuit on demand. In particular, we will outline how the coupler flux can be used to tune the interaction between the two qubits, and how noise in this flux leads to noise in the entangling parameter between the two qubits.

2.2 A Circuit Hamiltonian

The standard methods of circuit quantum electrodynamics [54] can be used to produce a Hamiltonian given the circuit described in Fig. 2-1. In this architecture, by design it is typical for there to be a significant separation of energy scales between the qubits and the coupler, and as such the Schrieffer-Wolff transformation [55] may be used

to generate a Hamiltonian for only the qubit degrees of freedom that are classically modulated by the coupler flux. This computation is mechanically simple but involved, and the procedure is outlined in detail in [53]. Our result is similar, and the parts relevant to this work may be summarized as,

$$H = \omega_1 a_1^\dagger a_1 - \frac{\eta_1}{2} a_1^\dagger a_1^\dagger a_1 a_1 + \omega_2 a_2^\dagger a_2 - \frac{\eta_2}{2} a_2^\dagger a_2^\dagger a_2 a_2 + g\left(a_1^\dagger a_2 + a_1 a_2^\dagger\right) \tag{2.2}$$

Here, a_i and $a_i^\dagger$ are the standard harmonic oscillator annihilation and creation operators for the i^{th} qubit, respectively. ω_1 and ω_2 are the qubit frequencies,

$$\omega_i \simeq 2\pi f_i^{\max} \sqrt{|\cos(\pi \Phi_i / \Phi_0)|}, \tag{2.3}$$

where $f_1^{\max} \simeq f_2^{\max} \simeq 6$GHz. η_1 and η_2 are the qubit nonlinearities, $\frac{\eta_1}{2\pi} \simeq \frac{\eta_2}{2\pi} \simeq$ 200MHz. g is the effective qubit-qubit interaction, and is given by, in the case where $\omega_1 = \omega_2 = \omega_q$,

$$g = \left(k_d - k^2 \frac{\omega_q^2}{\omega_c^2 - \omega_q^2}\right) \frac{\omega_q}{2}, \tag{2.4}$$

where ω_c is the coupler frequency, which takes the form of Eq. 2.3 with $f_c^{\max} \simeq 12$GHz. k_d and k are dimensionless coupling efficiencies that are calculated from the circuit capacitances shown in Fig. 2-1.

All in all, this Hamiltonian may be interpreted as two weakly anharmonic oscillators coupled by an interaction that swaps excitations from one to the other.

2.3 Flux-Tunable Coupling and Noise Sensitivity

From the form of Eq. 2.4, it is clear that it is possible (at least to the order of approximation employed here) to nullify the coupling between two qubits by tuning Φ_C. This occurs when,

$$k_d = k^2 \frac{\omega_q^2}{\omega_c^2 - \omega_q^2} \tag{2.5}$$

By design, this point is achieved near $\Phi_c = 0$, or $\omega_c = 2\pi f_c^{\max}$. The exact flux that nullifies the coupling is typically found experimentally. Conversely, at nonzero

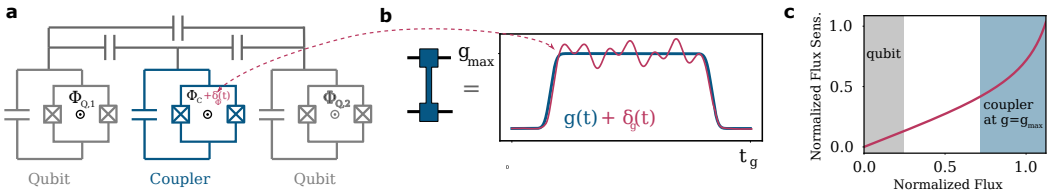

Figure 2-2: **Simple schematic of the tunable coupler transmon (a)** Simplified circuit diagram for two qubits and the tunable coupler. The qubit frequencies ω_j are modulated by changing $\Phi_{Q,j}$. The coupler frequency is changed significantly during two-qubit gates via Φ_C. **(b)** Schematic of the time-dependent coupling $g(t)$ enacted during two-qubit gates. The coupler flux noise $\delta_\Phi(t)$ generates coupling fluctuations $\delta_g(t)$ according to Eq. 2.7. **(c)** Flux sensitivity χ (Eq. 2.6) vs external flux. The qubits are generally operated at frequencies with much lower flux sensitivity than the coupler.

coupler flux, a finite coupling g develops between the two qubits, turning on the exchange interaction given by the $a_1^\dagger a_2 + a_1 a_2^\dagger$ term. Several two-qubit gates have been designed around this interaction and have achieved high fidelity [33, 34]. In particular, an iSWAP-like interaction is achieved when the two qubits are placed near resonance, $\omega_1 \simeq \omega_2$, and a non-zero g is developed. This work will focus on this type of interaction.

The focus of this work is not on the specifics of these iSWAP gates themselves, but rather on the effect of flux noise on g. The fluxes Φ_i are implemented by real electronics in the lab, and therefore they are not perfectly stable and contain a fluctuating component. This so-called flux noise is no stranger to superconducting circuit practitioners and has been studied at length [56, 57, 58, 59].

Transmon qubits are typically operated near zero flux at the so-called flux sweet spot, at which the qubit frequency is first-order insensitive to flux fluctuations [60]. Therefore, as long as our qubits don't move far from the sweet spot during gates, ω_q should remain relatively stable and should not induce fluctuations in g. We will not concern ourselves with the qubit fluxes any further in this work. However, to enact fast two-qubit gates, the coupler frequency must be lowered substantially from $\omega_{max} = 2\pi f_c^{\max}$, such that $\Phi_C/\Phi_0 \simeq 1/2$. This is illustrated in Fig. 2-2. This is far from the coupler's flux sweet spot, and fluctuations in ω_c may be significant. The

flux sensitivity of g, $\tilde{\chi}_\Phi$, is given by,

$$\tilde{\chi}_\Phi = \left|\frac{\partial g}{\partial \Phi}\right| = \frac{k^2\omega_q^3\omega_{\max}^2 \sin(\pi\Phi/\Phi_0)}{4\Phi_0\left(\omega_{\max}^2\cos(\pi\Phi/\Phi_0) - \omega_q^2\right)^2} \tag{2.6}$$

Solving the system of equations (2.4) and (2.3) for Φ and ω_c and substituting the result into Eq. (2.6) we obtain the desired relation between the flux sensitivity and g:

$$\tilde{\chi}_\Phi(g) = \frac{(k_d\omega_q - 2g)\sqrt{\omega_{\max}^4\left(k_d\omega_q - 2g\right)^2 - \omega_q^4\left(k_{qq}\omega_q - 2g\right)^2}}{4\Phi_0 k^2\omega_q^3}, \tag{2.7}$$

where $k_{qq} = k_d + k^2$ is the total coupling efficiency, which includes both direct and indirect interactions between the qubits. The flux sensitivity in (2.7) is positive since we are considering only those ω_c for which the indirect coupling prevails, i.e. according to Eq. (2.4) the value of g is negative; we also assume $\omega_c > \omega_q$. In the parameter range of interest for the experiment, and in particular, with the account taken of the smallness of the dimensionless parameter k, $\tilde{\chi}_\Phi(g)$ is extremely well approximated by a quadratic polynomial in g as,

$$\tilde{\chi}_\Phi(g) = \chi_\Phi^{(0)} + \chi_\Phi^{(1)}g + \chi_\Phi^{(2)}g^2 \tag{2.8}$$

Chapter 3

Measuring Noise in the Coupler

With an understanding of the physical origins of g-noise in hand, we now devise an experimental protocol for measuring it in the lab. Our approach is to reduce the two-qubit Hamiltonian of 2.2 to an effective two-level system, such that the multitude of techniques developed for studying single qubit dephasing can be transferred to this problem of studying g-noise. We will present this effective two-level system in section 3.1, and use it to devise g-noise metrology schemes in section 3.2. Then, in section 3.3 we will derive equations predicting the results of our measurements for general classical g-fluctuations, with integrals that we will solve for specific kinds of random processes in later chapters.

3.1 The Psuedo-Spin and g-Noise

One symmetry of the Hamiltonian 2.2 is that it commutes with $a_1^\dagger a_1 + a_2^\dagger a_2$, i.e it conserves the total number of excitations in the two non-linear oscillators. Therefore, the Hamiltonian is block-diagonal in the two-oscillator number basis. If we choose the single excitation basis, spanned by the states $|01\rangle$ and $|10\rangle$, we can re-write the Hamiltonian as,

$$H = \frac{1}{2}\left(\omega(t) + \delta\omega(t)\right)\sigma_z + \left(g(t) + \delta g(t)\right)\sigma_x \,, \tag{3.1}$$

where $\sigma_z = |01\rangle\langle 01| - |10\rangle\langle 10|$ and $\sigma_x = |01\rangle\langle 10| + |10\rangle\langle 01|$. Note that here $\omega(t)$ indicates the difference in the qubit frequencies, $\omega_1 - \omega_2$, while $g(t)$ and $\delta g(t)$ are the control and noise contributions to the inter-qubit coupling. Therefore, when operated in the single excitation subspace, our two-qubit system can be thought of as a single pseudo-spin.

During many types of two-qubit gates, the two qubits are on resonance, $\omega(t) = 0$. In this case, $\delta\omega(t)$ and $g(t) + \delta g(t)$ can be considered respectively as z and x components of an effective magnetic field. The Bloch vector of our effective two-level system undergoes Larmor precession around the instantaneous axis, which is almost parallel to the x-field, with the instantaneous Larmor frequency given by

$$\omega_L(t) \simeq 2g(t) + 2\delta g(t) + \frac{\delta\omega^2(t)}{4g(t)} \,. \tag{3.2}$$

From this, we can see that coupler noise will dominate during these resonant two-qubit gates: $\delta g(t)$ shows up to first order in the dynamics while $\delta\omega(t)$ only shows up to second-order and is suppressed by a factor of $g(t)$.

3.2 g-Noise Noise Spectroscopy Sequences

Understanding that $\delta\omega$ does not significantly affect the dynamics, an important point to realize about Eq. 3.1 is that it is, up to a rotation of the entire problem, completely equivalent to a model of classical fluctuations in the frequency of a single qubit. Using this equivalence, we can port all of the work that has been done in single qubit frequency noise characterization [35, 37, 38] over to our problem. In particular, we consider the traditional Ramsey [61] and Carr-Purcell-Meiboom-Gill (CPMG) [62, 63] sequences.

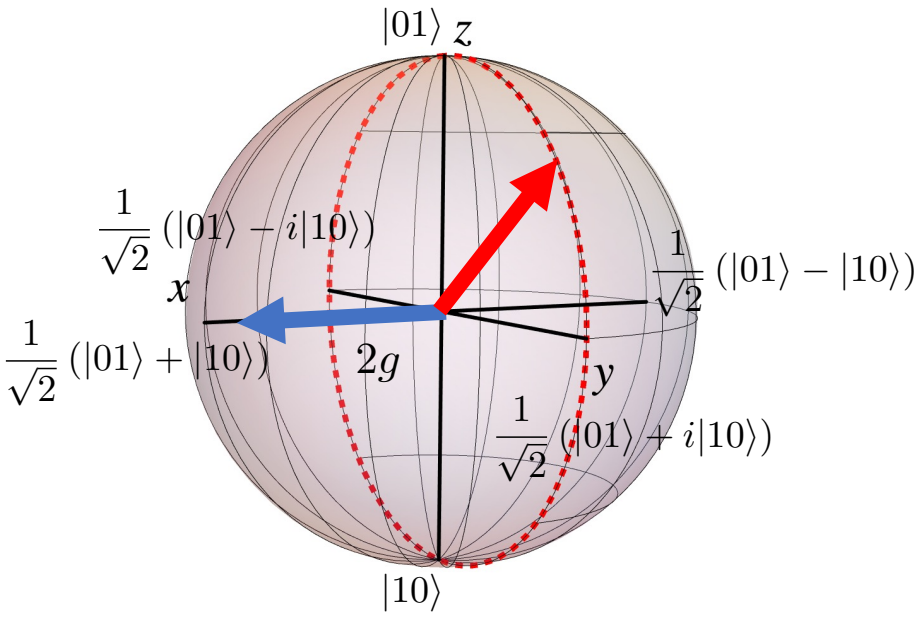

Figure 3-1: Schematic view of the post-selected Bloch vector (red arrow) trajectory (red dashed line) rotating around a fluctuating magnetic field with the mean magnitude $2g$ (blue arrow).

3.2.1 The Coupler Ramsey Sequence

The traditional Ramsey sequence is used to measure the energy level splitting of a two-level system, i.e ω in the following Hamiltonian,

$$H_{\text{ramsey}} = (\omega + \delta\omega(t))\sigma_z \tag{3.3}$$

To do this, the spin is initialized along the x-axis of the Bloch sphere via a $\pi/2$ pulse and is then allowed to process about the z-axis. After a duration t, the $\pi/2$ pulse is repeated, and the spin is measured in the z basis. Interference fringes will be observed in the probability of measuring the spin in the excited state vs t. ω can easily be extracted from these oscillations. The frequency noise term $\delta\omega$ leads to broadening of the observed fringes. Analyzing this broadening can serve as a primitive characterization of $\delta\omega$, as will be explored later in this work.

The *coupler Ramsey* sequence is a modification of the traditional sequence for characterizing g and δg in 3.1. Since g is aligned with the x-axis, we initialize our

pseudo-spin along the z-axis in the state $|01\rangle$ by exciting one of the physical qubits using a microwave pulse. The coupler is then tuned to develop a non-zero g, allowing the pseudo-spin to process about the x-axis for time t. The pseudo-spin is then measured in the z-basis, which corresponds to z-basis measurements on both of the physical qubits. In the same way as the traditional sequence, fringes in the probability of observing the state $|01\rangle$ can be analyzed to determine g, and broadening in the fringes contains some information about δg. Figure 3-3 (b) shows how we typically experimentally implement the coupler Ramsey sequence. As indicated, nonzero g is developed by repeatedly applying a precalibrated two-qubit gate, such that g is repeatedly pulsed from 0 to $g_{\max}$ (see Fig. 2-2). The duration of the experiment is determined by n, the number of two-qubit gates applied. A so-called continuous waveform (CW) experiment is also possible, in which g is kept at a constant value for the entire procession stage.

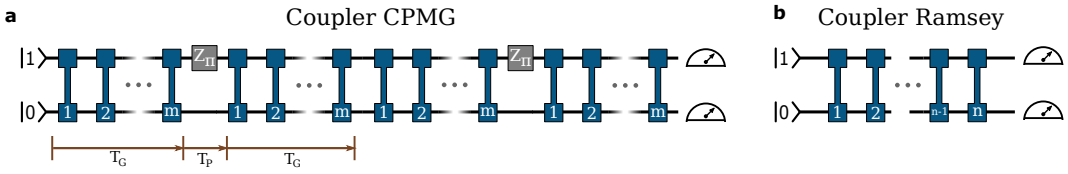

Figure 3-2: **Coupler CPMG and Ramsey sequences (a)** Circuit diagram showing the Coupler CPMG (Carr-Purcell-Meiboom-Gill) sequence. Shown here are $n = 2$ repetitions of a pulse sequence involving $2m$ two-qubit gates that are separated by a qubit frequency π pulse. The two-qubit gates serve to expose the qubits to g-noise, which is refocused by the frequency pulse. The decay of the pseudo-qubit $\langle\sigma_z\rangle$ observable is measured at the end of the circuit, which can be used to characterize the noise. **(b)** Circuit diagram showing the Coupler Ramsey sequence involving n two-qubit gates, which can be used to measure the response of the qubits to g-noise in the absence of refocusing pulses.

3.2.2 The Coupler CPMG Sequence

CPMG was originally a method of refocusing spins subject to fluctuating fields in NMR experiments and has since been widely employed as a method of characterizing and protecting qubits from frequency noise [37, 64, 65, 66]. The essence of the traditional CPMG sequence is to add evenly spaced σ_x π-pulses to the middle of the Ramsey sequence. These pulses serve to refocus $\delta\omega$ noise such that the qubit is only exposed to noise at a particular frequency, which overall improves coherence and allows the spectrum of the noise to be explicitly measured. These noise-filtering properties will be explored in greater depth later in this work.

As in the Ramsey case, the *coupler CPMG* sequence is simply an overall rotation of the traditional CPMG sequence. The π-refocusing pulses are about the z-axis of the pseudo-spin, which corresponds to a σ_z π pulse on one of the physical qubits. The experimental implementation of this sequence is shown schematically in Fig. 3-3 (a).

The coupler CPMG sequence has a few integer parameters. m is the number of g-pulses that occur before and after each z-pulse, and n is the total number of z-pulses in the experiment. This is shown for several values of m and n in Fig. 3-3.

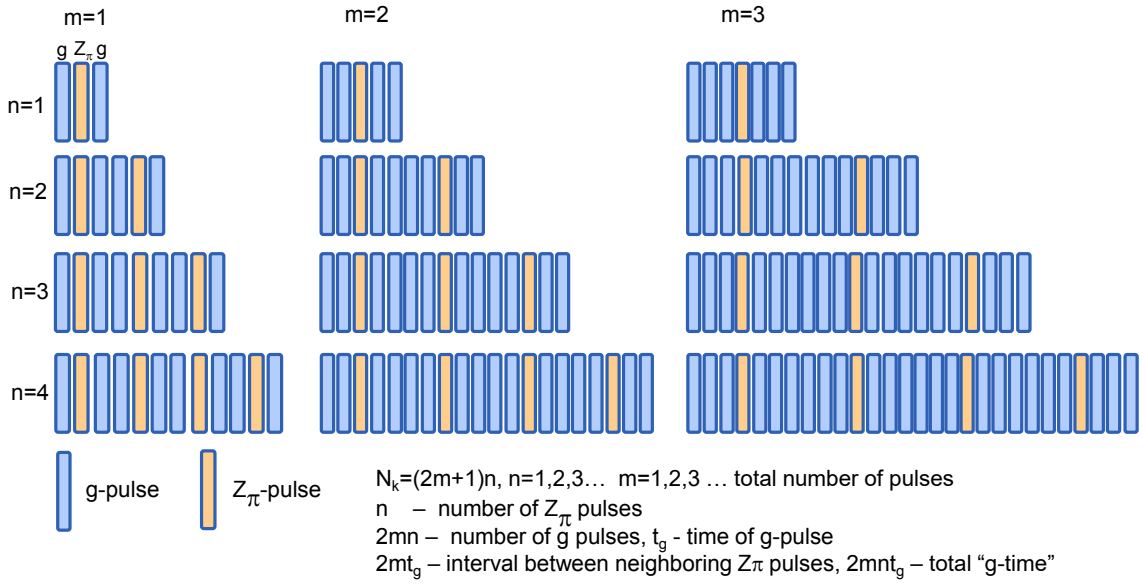

Figure 3-3: Examples of the coupler CPMG sequence for different values of n and m.

3.3 Stochastic Dynamics Under g-Noise

With these pulse sequences in hand, we now consider a generic model of the experimental observables under g-noise. First, we will examine the case of Coupler Ramsey decay under classical g-noise. If the frequencies of both qubits coincide, the complete Hamiltonian is,

$$H(t) = (g(t) + \lambda(t)\xi(t))\sigma_x \tag{3.4}$$

Here, 3.1 has been modified such that $\delta g(t) = \lambda(t)\xi(t)$. $\xi(t)$ is a real valued, unitless stochastic process and $\lambda(t)$ is the generally time-dependant amplitude of the g-noise. As described in the previous section, $g(t)$ is a periodic sequence of pulses with period T_{gate}. From the analysis completed in chapter 2, this also implies that $\lambda(t)$ is periodic with the same period. The associated propagator is,

$$U(t) = e^{-i\sigma_x G(t,0)} \tag{3.5}$$

$$G(t_2, t_1) = \int_{t_1}^{t_2} [g(\tau) + \lambda(\tau)\xi(\tau)]d\tau \tag{3.6}$$

If the system is initialized in the state $\rho(0) = |01\rangle\langle 01|$, the z-component of the one-excitation subspace Bloch vector $N(t) \equiv Tr[\sigma_z \rho(t)]$ is given by the expression

$$\begin{aligned} N(t) &= \langle 01|U(t)\rho(0)U^\dagger(t)|01\rangle - \langle 10|U(t)\rho(0)U^\dagger(t)|10\rangle \\ &= \text{Re}(e^{2i\int_0^t \lambda(\tau)\xi(\tau)d\tau} e^{2i\int_0^t g(\tau)d\tau}) \end{aligned} \tag{3.7}$$

The average Bloch vector component can be found by averaging Eq. 3.7 over noise trajectories. Taking into account that the measurement is done after an even number of g-gates, $\int_0^t g(t')dt' k\pi$, we have

$$\langle N(t)\rangle = \text{Re}\left(\chi(t) e^{2i\int_0^t g(\tau)d\tau}\right) \tag{3.8}$$

$$\chi(t) = \langle e^{2i\int_0^t \lambda(\tau)\xi(\tau)d\tau}\rangle \tag{3.9}$$

The Ramsey decay envelope is given by an integral over the random process ξ weighted

by λ. The form of this integral for different types of random processes will be explored in later chapters.

We can now consider the case of Coupler-CPMG decay. Here we apply a periodic sequence of σ_z gates to suppress the coupler noise. In the limit that the σ_z gates are very short, the Hamiltonian that describes the Coupler-CPMG reads:

$$H_{\mathrm{CPMG}} = H(t) - \frac{\pi}{2}\sigma_z \sum_k \delta\left[t - (k+1/2)T_C\right] \tag{3.10}$$

Here the period T_C is the duration of a sequence of $2m$ two-qubit gates. The pulses $\propto \sigma_z$ are the pulses of the difference of the qubit frequencies, and during these pulses in the experiment $g(t) = 0$, so that the coupled noise is not accumulated. As in the conventional CPMG, the first refocusing pulse is applied at $T_C/2$, and the measurement is at nT_C, that is, the time interval between the last refocusing pulse and the measurement is $T_C/2$.

The time evolution operator of the system is

$$U_{\mathrm{CPMG}}(nT_C, 0) = \mathcal{T} \exp\left[-i \int_0^{nT_C} dt H_{\mathrm{CPMG}}(t)\right] \tag{3.11}$$

($\mathcal{T}$ is the time ordering operator). The operator U_{CPMG} can be simplified if one takes into account that $\sigma_z\sigma_x = -\sigma_x\sigma_z$, and therefore $\sigma_z \exp[-i\int H(t)dt] = \exp[i\int H(t)dt]\sigma_z$. One can then use in Eq. (3.11) that $\exp(-i\pi\sigma_z/2) = -i\sigma_z$ and move in the time-ordered operator U_{CPMG} all σ_z at times $(2k+1)T_C$ to $(2k+2)T_C$ ($k = 0, ..., \lfloor (n-2)/2 \rfloor$; for odd $n-1$ the last σ_z is moved to nT_C). This gives

$$U_{\mathrm{CPMG}}(nT_C) = (-i)^{n-1} \exp\left[-i \int_0^{nT_C} h(t)H(t)\right], \tag{3.12}$$

where $h(t)$ is a filter function. It changes sign depending on t being in the interval preceded by an even or odd number of refocusing pulses,

$$h(t) = 1 + 2\sum_{m=1}^{n} (-1)^m \Theta[t - (m-1/2)T_C] \tag{3.13}$$

We now consider the expectation value of the z-component of the Bloch vector $N_{\mathrm{CPMG}}(nT_C) = \langle Tr[\sigma_z U_{\mathrm{CPMG}}(nT_C)\rho(0)U^{\dagger}_{\mathrm{CPMG}}(nT_C)]\rangle$. Taking into account that $[H(t), H(t')] = 0$, we can write the general expression for the observable in the form similar to that in the absence of the CPMG pulses

$$N_{\mathrm{CPMG}}(nT_C) = \mathrm{Re}\left(\chi_{\mathrm{CPMG}}(nT_C)\right) \tag{3.14}$$

where

$$\chi_{\mathrm{CPMG}}(t) = \langle e^{2i\int_0^t h(\tau)\lambda(\tau)\xi(\tau)d\tau}\rangle \tag{3.15}$$

Chapter 4

Gaussian g-Noise

With a scheme in place for measuring g-noise, we now turn to understanding how different types of noise will manifest themselves in our experimental measurements. We begin with models of *Gaussian* random processes, which have historically been very useful in experimental quantum computing. In particular, we will attack the integrals given by Eqs. 3.9 and 3.15 in the case where $\xi(t)$ is Gaussian. Due to the ubiquity of Gaussian random processes in experiments, many of the results shown here are known. However, a detailed knowledge of these calculations was required to interpret the experimental results to be shown later in this work, so our independent versions of them are presented in detail here.

The main technical goal of this chapter is to establish what kind of signals we should expect to receive from our coupler Ramsey and CPMG measurements in the case of Gaussian g fluctuations. As such, we will proceed by first briefly reviewing the definition of Gaussian noise in section 4.1, and then leveraging this definition and other techniques to solve the aforementioned integrals in section 4.2 . In section 4.3, we will study the properties of these solutions and argue that it is very difficult for any Gaussian noise to produce non-smooth decay curves in a CPMG experiment. This provides a simple prediction that can be compared with experimental data in later sections.

4.1 What a Gaussian Process?

A random process is called Gaussian if any bounded integral over the process produces a Gaussian random variable,

$$X(t) = \int_0^t g(\tau)x(\tau)d\tau \tag{4.1}$$

for any $g(\tau)$ satisfying,

$$\int_0^t |g(\tau)|d\tau < \infty \tag{4.2}$$

An important consequence of this is that any Gaussian random process is completely described by its second-order statistics (in analogy to how a Gaussian random variable is completely described by its covariance matrix). As such, zero-mean fluctuations that couple weakly to a dynamic system tend to appear to be Gaussian, as the leading contribution is second order. Therefore, we can cover significant experimentally relevant ground by studying how Gaussian noise processes affect our pulse sequences.

4.2 Coupler Ramsey and CPMG Under Gaussian g-Noise

if $\xi(t)$ is Gaussian noise, decay functions $\chi(t)$ or $\chi_{\mathrm{CPMG}}(t)$, as in Eq. (3.15), are given by

$$\chi(t) = \langle e^{2i\int_0^t h(\tau)\xi(\tau)d\tau}\rangle = e^{-\Gamma(t)} \tag{4.3}$$

$$\Gamma(t) = 2\int_0^t d\tau_1 \int_0^t d\tau_2 h(\tau_1)h(\tau_2)\langle\xi(\tau_1)\xi(\tau_2)\rangle \tag{4.4}$$

For stationary $\xi(t)$ the correlator depends only on the time difference, $\langle\xi(\tau_1)\xi(\tau_2)\rangle = c(\tau_1 - \tau_2)$, and then $\Gamma(t)$ can be expressed in terms of the noise power spectrum $S(\omega) = S(-\omega)$,

$$\Gamma(t) = 2\int_0^\infty \frac{S(\omega)}{\pi}F(\omega,t)d\omega \tag{4.5}$$

$$c(\tau_1 - \tau_2) = \int_{-\infty}^{\infty} \frac{S(\omega)}{2\pi} e^{i\omega(\tau_1 - \tau_2)} d\omega \tag{4.6}$$

$$F(\omega, t) = \int_0^t h(\tau_1) e^{i\omega\tau_1} d\tau_1 \int_0^t h(\tau_2) e^{-i\omega\tau_2} d\tau_2 \tag{4.7}$$

In the literature, $F(\omega, t)$ is often referred to as a "filter function" [38]. In the case of Coupler Ramsey measurement $h(t) = 1$, and $F(\omega, t)$ is

$$F(\omega, t) = 4\frac{\sin^2\left(\frac{\omega t}{2}\right)}{\omega^2} \tag{4.8}$$

In the case of 1/f noise $S(\omega) = \frac{\lambda^2}{\omega}$, and $\Gamma(t)$ is

$$\Gamma(t) = -\frac{2\lambda^2\left(-1 + \cos\left(\omega_m t\right) + \omega_m t(\omega_m t\,\mathrm{Ci}(\omega_m t) - \sin\left(\omega_m t\right))\right)}{\pi\omega_m^2} \tag{4.9}$$

$$\mathrm{Ci}(z) = -\int_z^{\infty} \frac{\cos\left(t\right)}{t} dt \tag{4.10}$$

where ω_m is the low-frequency cutoff of $S(\omega)$.

In the experimentally relevant limit where $\omega_m t$ is small,

$$\Gamma(t) \approxeq \frac{\lambda^2 t^2}{\pi}(3 - 2\gamma_{\mathrm{Euler}} + 2\ln\left(\frac{1}{\omega_m t}\right)) \tag{4.11}$$

Since $\ln\left(\frac{1}{\omega_m t}\right)$ is a slowly changing function, Eq. 4.11 produces approximately Gaussian decay,

$$\chi(t) \approxeq e^{-\Gamma_G t^2} \tag{4.12}$$

$$\Gamma_g \propto \lambda^2 \tag{4.13}$$

We can now discuss the case of decay in the presence of CPMG filtering. Let us consider a Gaussian noise with the power spectral density equal to that of a single RTN fluctuator (to be elaborated on later, see chapter 5):

$$S(\omega) = \frac{4\lambda^2\gamma}{\omega^2 + 4\gamma^2} \tag{4.14}$$

Here, the new parameter γ is the timescale of the RTN fluctuations. For an arbitrary CPMG sequence with n echo pulses the decay envelope function is given by the standard expression:

$$\chi(n, T_C) = e^{-\Gamma(n,T_C)}, \tag{4.15}$$

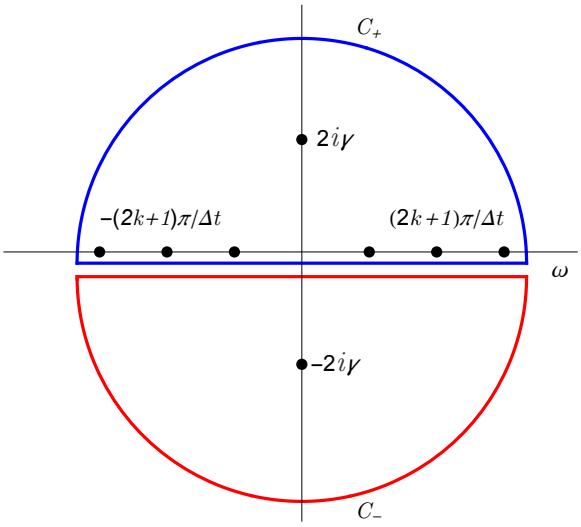

Figure 4-1: Integration contours for computing $\Gamma(n, T_C = \Delta t)$

The filter function in this case is:

$$F(n, \omega T_C) = \frac{1}{\omega^2}\left(1 - \frac{1}{\cos(\omega T_C/2)}\right)^2 \times \begin{cases} \sin^2(n\omega T_C/2) & \text{if } n \text{ even} \\ \cos^2(n\omega T_C/2) & \text{if } n \text{ odd} \end{cases} \tag{4.16}$$

Here T_C is the time interval between two consecutive π-pulses of the n-pulse sequence such that the total sequence time $t = nT_C$. Using Eqs. (4.14) and (4.16) we can split the integral in Eq. (4.5) as follows:

$$\Gamma(n, T_C) = I_0(T_C) - \frac{1}{2}(-1)^n \left(I_+(n, T_C) + I_-(n, T_C)\right), \tag{4.17}$$

where

$$I_0(T_C) = \frac{1}{2\pi}\int_{-\infty}^{\infty} d\omega \left(\frac{16\lambda^2\gamma}{\omega^2\left(4\gamma^2+\omega^2\right)} + \frac{16\lambda^2\gamma\left(\left(-1+\sec\left(\omega T_C/2\right)\right)^2-1\right)}{\omega^2\left(4\gamma^2+\omega^2\right)} \right) \tag{4.18}$$

$$I_+(n,T_C) = \frac{1}{2\pi}\int_{-\infty}^{\infty} d\omega \frac{16\lambda^2\gamma e^{in\omega T_C}\left(-1+\sec\left(\omega T_C/2\right)\right)^2}{\omega^2\left(4\gamma^2+\omega^2\right)} \tag{4.19}$$

$$I_-(n,T_C) = \frac{1}{2\pi}\int_{-\infty}^{\infty} d\omega \frac{16\lambda^2\gamma e^{-in\omega T_C}\left(-1+\sec\left(\omega T_C/2\right)\right)^2}{\omega^2\left(4\gamma^2+\omega^2\right)} \tag{4.20}$$

The integrands in Eqs. (4.18)-(4.20) have infinite series of poles at frequencies $\omega_k = \pm(2k+1)\pi/T_C$ and additional two poles at $\pm 2i\gamma$ (see Fig 4-1). To evaluate the integrals I_+ and I_- we use the contours C_+ and C_- respectively, as shown in Fig. 4-1, and obtain:

$$I_+(n,T_C) = \sum_{k=0}^{\infty} \frac{(-1)^{n+1}32n\lambda^2 T_C}{\pi^2\gamma(2k+1)^2\left(1+(2k+1)^2\pi^2/(2\gamma\Delta t)^2\right)} - \frac{4\lambda^2 e^{-2n\gamma T_C}\sinh^4\left(\gamma T_C/2\right)}{\gamma^2\cosh^2(\gamma T_C)} \tag{4.21}$$

and

$$I_-(n,T_C) = -\frac{4\lambda^2 e^{-2n\gamma T_C}\sinh^4\left(\gamma T_C/2\right)}{\gamma^2\cosh^2(\gamma T_C)} \tag{4.22}$$

The integral I_0 can be computed by integrating the first term in Eq. (4.18) along the horizontal line proximate to the real axis and lying in the lower half-plane. Then we can close the contour (C_-) in the lower half-plane to evaluate the remaining integral along this contour. This yields:

$$I_0(n,T_C) = -\frac{4\lambda^2\sinh^4\left(\gamma T_C/2\right)}{\gamma^2\cosh^2(\gamma T_C)} \tag{4.23}$$

After evaluating the sum in Eq. (4.21) and substituting Eqs. (4.21)- (4.23) into Eq. (4.17) we finally obtain:

$$\Gamma(n,T_C) = \frac{2\lambda^2 n}{\gamma^2}\left(\gamma T_C - \tanh(\gamma T_C)\right) - \delta\Gamma(n,T_C), \tag{4.24}$$

where

$$\delta\Gamma(n,T_C)=\frac{8\lambda^2 e^{-n\gamma T_C}\sinh^4(\gamma T_C/2)}{\gamma^2\cosh^2(\gamma T_C)}\times\begin{cases}\sinh(n\gamma T_C) & \text{if } n \text{ even}\\ \cosh(n\gamma T_C) & \text{if } n \text{ odd}\end{cases} \tag{4.25}$$

Eqs. (4.24) and (4.25) are exact for any Gaussian noise with a Lorentzian power spectrum and for any n. They also match the weak-coupling limit of the CPMG formula for a non-Gaussian noise induced by a single random telegraph noise source. For large n only the first term, proportional to n is important. This term describes the well-known CPMG exponential decay for large n, with $\Gamma(n,T_C)\propto n$.

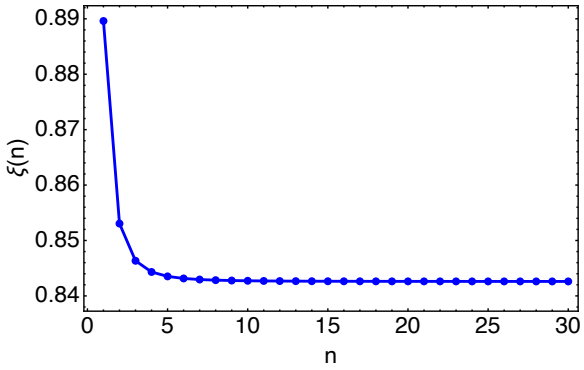

Figure 4-2: Dependence of $\Gamma'(n,T_C)$ on n for $1/f$ noise

For $1/f$-noise with $S(\omega)=\frac{\lambda^2}{\omega}$ we find

$$\frac{\partial\Gamma(n,T_C)}{\partial n}=2T_C^2\lambda^2\xi(n)\propto\omega_c^{-2}, \tag{4.26}$$

where

$$\xi(n)=\int_0^\infty\left(\frac{x-\tanh(x)}{x^3}+\frac{8e^{-2nx}\mathrm{sech}^2(x)\sinh^4\left(\frac{x}{2}\right)}{x^2}\right)dx \tag{4.27}$$

only weakly depends on n (see Fig. 4-2) and quickly saturates at

$$\xi(\infty)=\int_0^\infty\left(x-\tanh(x)\right)/x^3=0.8525 \tag{4.28}$$

Therefore, letting $T_C=\frac{t}{n}$,

$$\Gamma(t)\approxeq\frac{2t^2\lambda^2\xi(n)}{n} \tag{4.29}$$

This describes Gaussian decay with a rate inversely proportional to n. Therefore, under a Gaussian noise model, we would expect that increasing the number of echo pulses that occur in time t should always increase the amount of noise protection.

4.3 Gaussian Noise Leads to Smooth Decay

A characteristic feature of all of the solutions presented in the previous section is that they are smooth: the solutions do not oscillate or step. This section will try to argue that this is a generic feature of the Gaussian noise generally seen in superconducting devices. To start, consider that the time derivative of the decay envelope under Gaussian noise is given by,

$$\frac{d\chi(t)}{dt} = -e^{-\Gamma(t)}\frac{d\Gamma(t)}{dt} \tag{4.30}$$

The first two terms in this expression are always positive for non-zero $S(\omega)$, as $F(\omega, t)$ is non-negative. Therefore, if zeros are to be present in the derivative of $\chi(t)$, the following condition must be met,

$$0 = \frac{d\Gamma(t)}{dt} = \int_0^\infty S(\omega)\frac{dF(\omega,t)}{dt}d\omega \tag{4.31}$$

For an even CPMG sequence, $\frac{dF(\omega,t)}{dt}$ is given by,

$$\frac{dF(\omega,t)}{dt} = \frac{\sin\left(\frac{t\omega}{2}\right)\left(\sec\left(\frac{t\omega}{2n}\right)-1\right)\left(n\cos\left(\frac{t\omega}{2}\right)\left(\sec\left(\frac{t\omega}{2n}\right)-1\right)+\sin\left(\frac{t\omega}{2}\right)\tan\left(\frac{t\omega}{2n}\right)\sec\left(\frac{t\omega}{2n}\right)\right)}{n\omega} \tag{4.32}$$

where $F(\omega, t)$ was obtained by substituting $T_C = \frac{t}{n}$ into equation 4.16. Since $F(\omega, t)$ has the form of a product of ω^{-2} and a function of $\omega t/n$, the derivative $dF/dt \propto (\omega n)^{-1}$. For $n = 2$, the function dF/dt has zeros at,

$$\omega = \frac{8\pi m}{t},\ \frac{4\left(\frac{-2\pi}{3}+2\pi m\right)}{t},\ \frac{4\left(\frac{2\pi}{3}+2\pi m\right)}{t},\ m \in \mathbb{Z} \tag{4.33}$$

The first positive zero is at $\omega_0 = \frac{8\pi}{3t_z}$, and $F(\omega, t_Z) > 0$ for $\omega < \omega_0$, as shown in figure 4-3. It is clear from figure 4-3 that for there to be a single zero in $\frac{dF(\omega,t)}{dt}$ during

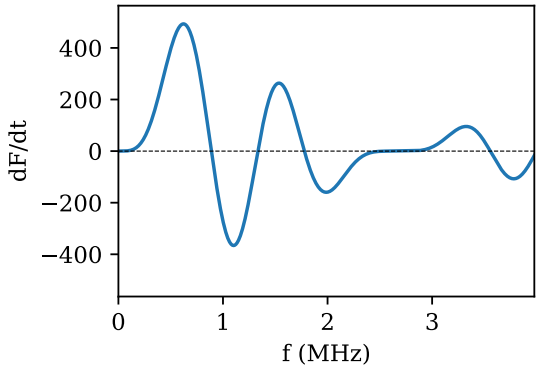

Figure 4-3: Plot of $\frac{dF(\omega,t)}{dt}$ for n=2 and $t_z = 1500$ns, $f = \frac{\omega}{2\pi}$.

a typical CPMG experiment, say at $t = t_z \approxeq 1500$ns, the noise must have much more power at frequencies larger than $\omega_0 \approxeq 1$MHz than at low frequencies. This requirement directly contradicts modern experimental observations of flux noise in SQUID-based devices [67, 68, 69, 70] which find $1/f$ noise over a range extending well past 1MHz. Additionally, this high-frequency power must be concentrated in the regions of frequency where $\frac{dF(\omega,t)}{dt}$ is positive, which would mean $S(\omega)$ could not be smooth on the MHz scale. These requirements are very contrived, and as such it seems likely that any non-smooth features observed in experimental data are more likely to be the results of non-Gaussian contributions in the noise.

Chapter 5

Telegraph g-Noise

While Gaussian models have been incredibly successful at reproducing the results of many experiments, there is some reason to believe that non-Gaussian models may be useful for understanding g-noise. As discussed in section 2.2, the coupler is moved far from the flux sweet spot during two-qubit gates, and flux noise couples much more strongly to the system than it ever does in the case of single-qubit frequency control. Therefore, the leading order approximation that leads to Gaussian behavior may break down revealing signatures of non-Gaussianity.

Here, we consider non-Gaussian random telegraph noise (RTN). RTN models a switching process that instantaneously jumps between two states. As will be discussed later, $1/f$ noise, which is ubiquitous in solid state systems [71, 72, 73, 74], is commonly thought of as being the result of a superposition of many weak RTN sources. As such, it is reasonable to think that as coupling to the noise is increased the most strongly coupled fluctuators in the ensemble could enter the non-Gaussian regime, and become visible in the data. Here this possibility will be explored.

We will begin in section 5.1 by reviewing the details of RTN, and by connecting it to the $1/f$ noise discussed in the previous chapter in section 5.2. Section 5.3 will then present several different ways to evaluate the integrals given in Eqs. 3.9 and 3.15 in the case of RTN, producing closed-form expressions for the experimental observables in the case that fluctuations in g are dominated by RTN. Development of these expressions is critical, as in later chapters they will be used to interpret and fit

experimental data. Section 5.4 explores an implication of non-Gaussian noise on error mitigation, namely that unlike in the Gaussian case, "spin echo" techniques can't be easily used to protect information when the noise is strong.

5.1 Random Telegraph Noise

Here the statistics of single RTN processes are briefly reviewed. The RTN process is a Markovian process in which the variable $\xi(t)$ switches randomly between two values $\xi(t) = \pm 1$ with an average rate γ [75]. We assume that the noise is symmetric, i.e. the probabilities of switching "up" and "down" are equal. The number of switches during the time interval $(0, t)$ is described by a Poisson distribution. As such, we can obtain the differential equation for the probability distribution of $\xi(t)$:

$$\frac{d}{dt}P^{\xi}_{\sigma_0,\sigma}(t) = -\gamma(P^{\xi}_{\sigma_0,\sigma}(t) - P^{\xi}_{\sigma_0,-\sigma}) = -\gamma(2P^{\xi}_{\sigma_0,\sigma}(t) - 1) \tag{5.1}$$

Here $P^{\xi}_{\sigma_0,\sigma}(t)$ is the probability that the discrete variable $\xi(t)$ assumes the value σ conditioned on initial value $\xi(0) = \sigma_0$ and we assumed that $P_{\sigma_0,+}(t) + P_{\sigma_0,-}(t) = 1$. For example, $P^{\xi}_{+-}(t)$ is the probability that the variable $\xi(t) = -1$ conditioned upon $\xi(0) = +1$. Eq. (5.1) can be readily solved, and we obtain:

$$P^{\xi}_{\sigma_0,\sigma}(t) = \left(\delta_{\sigma_0,\sigma} - \frac{1}{2}\right)e^{-2\gamma t} + \frac{1}{2} \tag{5.2}$$

The two-point time-domain correlator of RTN and its Fourier transform can be obtained as well:

$$\langle \xi(t)\xi(0)\rangle = e^{-2\gamma|t|} \tag{5.3}$$

and

$$S(f) = \int_{-\infty}^{\infty} dt e^{i2\pi f t}\langle \xi(t)\xi(0)\rangle = \frac{\gamma}{\pi^2 f^2 + \gamma^2} \tag{5.4}$$

There also exists a useful recurrence relationship between higher-order correlators and the second-order correlator [75],

$$\langle \xi(t_1) \dots \xi(t_n) \rangle = \langle \xi(t_1)\xi(t_2) \rangle \langle \xi(t_3) \dots \xi(t_n) \rangle \tag{5.5}$$

or $t_1 \geq t_2 > t_3, ..., t_n$.

5.2 $1/f$ Spectra from Telegraph Fluctuators

Consider the case of the noise that drives the qubit coming from the coupling to many independent random telegraph fluctuators. If the probability densities of the coupling strength λ and of the inverse correlation times of the fluctuators γ are $g_\lambda(\lambda)$ and $g_\gamma(\gamma)$, respectively, the power spectrum of the noise is,

$$S(f) = \int_{-\infty}^{\infty} d\lambda \, g_\lambda(\lambda) \int_{-\infty}^{\infty} d\gamma \, g_\gamma(\gamma) \frac{\lambda^2 \gamma}{\pi^2 f^2 + \gamma^2} \tag{5.6}$$

In the particular case where λ is the same for all fluctuators, $g_{\lambda_0}(\lambda_0) = \delta(\lambda_0 - \lambda)$, and γ has a log-uniform density of states,

$$g_\gamma(\gamma) = \begin{cases} \frac{1}{(\ln(\gamma_{\max}) - \ln(\gamma_{\min}))\gamma}, & \gamma_{\min} < \gamma < \gamma_{\max} \\ 0, & \text{otherwise} \end{cases} \tag{5.7}$$

$S(f)$ takes the form,

$$S(f) = \lambda^2 \frac{\cot^{-1}\left(\frac{f\pi}{\gamma_{\max}}\right) - \cot^{-1}\left(\frac{f\pi}{\gamma_{\min}}\right)}{f\pi\left(\ln(\gamma_{\max}) - \ln(\gamma_{\min})\right)} \tag{5.8}$$

When $\gamma_{\min} << f << \gamma_{\max}$, the numerator is well approximated by $\frac{\pi}{2}$, and the noise spectrum is approximately $S(f) = A/f$. It should be noted that there are many possible other choices of $g_\lambda(\lambda)$ and $g_\gamma(\gamma)$ that yield a similar result.

5.3 Coupler Ramsey and CPMG Under Telegraph Noise

Here we derive the expected decay envelopes for the Ramsey and CPMG sequences in the case of non-Gaussian RTN. We will demonstrate two different ways the solution can be reached. The first involves direct evaluation of the integrals in 3.9 and 3.15. This method is the most straightforward to understand for the simple case. The second method uses an identity for random processes with exponential correlators to reduce the stochastic dynamics to higher dimensional deterministic ODEs. This method is useful if one wants to add things to the model (such as single qubit T1 and T2 decay) that make the exact solution of the deterministic dynamics impossible.

5.3.1 Solutions via Direct Averaging

Here, we will derive the decay envelopes for the Ramsey and CPMG sequences under RTN. In the case of the Ramsey sequence, the integral 3.9 can be evaluated by expanding the functional $\chi(t)$ in a time-ordered Taylor series

$$\chi(t) = \sum_{k=0}^{\infty} (2i)^k \int_0^t dt_1 \int_0^{t_1} dt_2 \cdots \int_0^{t_{k-1}} dt_k \langle \xi(t_1) \dots \xi(t_k) \rangle \lambda(t_1) \dots \lambda(t_k) \tag{5.9}$$

In the considered problem $\lambda(t)$ is a periodic function of time. The typical period is the periodicity of the gate (moreover, $\lambda(t)$ is very nonsinusoidal, for much of the gate duration it is constant). The period of $\lambda(t)$ is much shorter than the typical time on which $\chi(t)$ varies. Therefore the major contribution to $\chi(t)$ comes from the term in $\lambda(t)$ that is independent of time. A justification of approximating $\lambda(t)$ by a constant can be done using the master equation formulation discussed in the next section. One can see there that the fast-oscillating terms in $\lambda(t)$ lead to fast-oscillating terms in the density matrix, which are small.

For $\lambda(t) \equiv \lambda = \frac{1}{t_g} \int_0^{t_g} \lambda(\tau) d\tau$ we can use the recurrence relation for the moments given in Eq. 5.5 to find a second order linear differential equation for $\chi(t)$,

$$\frac{d^2\chi(t)}{dt^2} + 2\gamma\frac{d\chi(t)}{dt} + 4\lambda^2\chi(t) = 0 \tag{5.10}$$

We can infer the initial conditions $\chi(0) = 1$ and $\chi'(0) = 0$ from Eq. 5.9. Then

$$\chi(t) = e^{-\gamma t}\left(\cosh(t\Omega) + \frac{\gamma\sinh(t\Omega)}{\Omega}\right) \tag{5.11}$$

$$\Omega = \sqrt{\gamma^2 - 4\lambda^2} \tag{5.12}$$

There are several ways to calculate the decay envelope in the CPMG case (3.15). They take advantage of $\xi(t)$ being a Markov random process and of the property (5.5). Here we start by employing time-ordered expansion of the telegraph noise to find an integrodifferential equation for $\chi_{\mathrm{CPMG}}(t)$,

$$\frac{d\chi_{\mathrm{CPMG}}(t)}{dt} = -4\lambda(t)h(t)\int_0^t e^{-2\gamma(t-t_1)}\lambda(t_1)h(t_1)\chi_{\mathrm{CPMG}}(t_1)dt_1 \tag{5.13}$$

We define $\Lambda(t)$,

$$\Lambda(t) = 2\int_0^t e^{-2\gamma(t-t_1)}\lambda(t_1)h(t_1)\chi_{\mathrm{CPMG}}(t_1)dt_1 \tag{5.14}$$

and arrive at the system of equations,

$$\begin{aligned}\frac{d}{dt}\begin{pmatrix}\chi_{\mathrm{CPMG}}(t)\\ \Lambda(t)\end{pmatrix} =& A(t)\begin{pmatrix}\chi_{\mathrm{CPMG}}(t)\\ \Lambda(t)\end{pmatrix}\\ A(t) =& \begin{pmatrix}0 & -2\lambda(t)h(t)\\ 2\lambda(t)h(t) & -2\gamma\end{pmatrix}\end{aligned} \tag{5.15}$$

Given that we consider the case $\lambda(t)$=const and $h(t) = \pm 1$, the solution of Eq. (5.15) can be obtained using the transfer matrix approach based on the piece-wise solution within an interval where $h(t)$ =const.

For $h = 1$ we have

$$\begin{pmatrix} \chi_{\mathrm{CPMG}}(t) \\ \Lambda(t) \end{pmatrix} = \hat{X}_{h=1}(t - t_1) \begin{pmatrix} \chi_{\mathrm{CPMG}}(t_1) \\ \Lambda(t_1) \end{pmatrix},$$

$$\hat{X}_{h=1}(t) = e^{-\gamma t} \begin{pmatrix} \cosh(\Omega t) + \frac{\gamma}{\Omega}\sinh(\Omega t) & -\frac{2\lambda \sinh(\Omega t)}{\Omega} \\ \frac{2\lambda \sinh(\Omega t)}{\Omega} & \cosh(\Omega t) - \frac{\gamma}{\Omega}\sinh(\Omega t) \end{pmatrix}, \tag{5.16}$$

where Ω is given by Eq. 5.12.

The solution of Eq. (5.15) for $h = -1$ has the same form, except that $X_{h=1}$ has to be replaced with $\hat{X}_{h=-1}$. The expression for $\hat{X}_{h=-1}$ can be obtained from Eq. (5.16) by replacing $\lambda \to -\lambda$. Alternatively, it can be written as

$$\hat{X}_{h=-1}(t) = \hat{Z}\hat{X}_{h=1}(t)\hat{Z}, \quad \hat{Z} = \begin{pmatrix} 1 & 0 \\ 0 & -1 \end{pmatrix} \tag{5.17}$$

The introduction of the matrix $\hat{Z}$ and the form of the solution for $h = \pm 1$ allows us to write the expression for the function $\chi_{\mathrm{CPMG}}(nT_C)$ in the form

$$\chi_{\mathrm{CPMG}}(nT_C) = \begin{pmatrix} 1 & 0 \end{pmatrix} \hat{Z}^{\,(n \bmod 2)} \left(\hat{X}_{h=1}(T_C/2)\hat{Z}\hat{X}_{h=1}(T_C/2) \right)^n \begin{pmatrix} 1 \\ 0 \end{pmatrix} \tag{5.18}$$

We have

$$\hat{X}_{h=1}(T_C/2)\hat{Z}\hat{X}_{h=1}(T_C/2) = e^{-\gamma T_C} \begin{pmatrix} (\gamma/\Omega)\sinh \Omega T_C + q & -(4\lambda\gamma/\Omega^2)\sinh^2(\Omega T_C/2) \\ (4\lambda\gamma/\Omega^2)\sinh^2(\Omega T_C/2) & (\gamma/\Omega)\sinh \Omega T_C - q \end{pmatrix}, \tag{5.19}$$

where

$$q = \frac{-4\lambda^2}{\Omega^2} + \frac{\gamma^2 \cosh(\Omega T_C)}{\Omega^2} \tag{5.20}$$

The matrix (5.19) is not skew-Hermitian, although the off-diagonal matrix elements have opposite signs, since Ω is either real or imaginary. Therefore its eigenvectors are

not orthogonal.

The eigenvalues of the matrix XZX are $-e^{-\alpha}$ and e^{α} where α is a solution of the equation

$$\sinh\alpha = \frac{\gamma}{\Omega}\sinh\Omega T_C \tag{5.21}$$

The expression for χ_{CPMG} is then easily found,

$$\chi_{\mathrm{CPMG}}(nT_C) = \begin{cases} e^{-n\gamma T_C}\left(q\frac{\cosh(n\alpha)}{\cosh(\alpha)} + \sinh(n\alpha)\right), & \text{n odd} \\ e^{-n\gamma T_C}\left(q\frac{\sinh(n\alpha)}{\cosh(\alpha)} + \cosh(n\alpha)\right), & \text{n even} \end{cases} \tag{5.22}$$

These results are similar to some of the expressions in [76, 77, 78, 79], but have been arranged into an algebraically simpler form.

It is clear how to extend the results to a superposition of independent RTN processes. For example, in the case of CPMG evolution,

$$\begin{aligned} \chi_{\mathrm{CPMG}}(t) =& \langle e^{2i\int_0^t h(\tau)\sum_k \lambda_k(\tau)\xi_k(\tau)d\tau}\rangle \\ =& \prod_k \langle e^{2i\int_0^t h(\tau)\lambda_k(\tau)\xi_k(\tau)d\tau}\rangle \\ =& \prod_k \chi^{(k)}_{\mathrm{CPMG}}(t) \end{aligned} \tag{5.23}$$

with $\chi^{(k)}_{\mathrm{CPMG}}(nT_C)$ given by Eq. (5.22) for the parameters γ, λ referred to the kth fluctuator.

If we set in Eq. (5.23) $h(t) = 1$, it describes the result in the absence of refocusing pulses.

5.3.2 Solutions via the Shapiro-Loginov Formula

The direct averaging approach used in the previous section is useful when a simple, closed-form solution for single trajectories of the noise is available. When this is not possible, other techniques must be used. One example of such a technique is the Shapiro-Loginov formula [80], which is valid for random processes with exponential correlators:

$$\langle \xi(t) \frac{d}{dt} R[\xi(t), t] \rangle = \frac{d}{dt} \langle \xi(t) R[\xi(t), t] \rangle + 2\gamma \langle \xi(t) R[\xi(t), t] \rangle \tag{5.24}$$

Here $R[\xi(t), t]$ is any functional of all histories $\{\xi(t'), t' \leq t\}$ that lead to value $\xi(t') = \xi(t)$ at $t' = t$ and the angular brackets mean averaging over all possible noise instances.

First, we consider the case of Coupler Ramsey decay. Let us write the Liouville - Von Neumann equation for the evolution of a density matrix of a qubit under a single source of the telegraph noise, and average over the noise instances using the Shapiro-Loginov formula. We write this equation in the vectorized form, which for a two-level system is a well-known Bloch equation for three components of the Bloch vector. For a two-qubit system in a single excitation subspace the x,y and z components are respectively: $P(t) = \langle 01|\rho|10\rangle + \langle 10|\rho|01\rangle$, $Q(t) = i(\langle 01|\rho|10\rangle - \langle 10|\rho|01\rangle)$ and $N(t) = \langle 01|\rho|01\rangle - \langle 10|\rho|10\rangle$. The Bloch equation reads:

$$\dot{\rho}(t) = (L_q(t) + \lambda(t)\xi(t)L_x)\rho(t) \tag{5.25}$$

where

$$L_q(t) = \begin{pmatrix} 0 & \omega(t) & 0 \\ -\omega(t) & 0 & g(t) \\ 0 & -g(t) & 0 \end{pmatrix} \tag{5.26}$$

is the regular part of the Liouvillian with $\omega(t)$ and $g(t)$ being the detuning and coupling between the qubits, respectively. The second term represents a stochastic part of the Liouvillian and describes the coupling of the qubit with the noise of amplitude $\lambda(t)$. The operator

$$L_x = \begin{pmatrix} 0 & 0 & 0 \\ 0 & 0 & 1 \\ 0 & -1 & 0 \end{pmatrix} \tag{5.27}$$

represents the noise coupling. The important property of the telegraph noise is that $\xi^2(t) = 1$, which substantially simplifies calculations. The second simplification comes from the Shapiro-Loginov formula. As a first step, we average the Liouville equation

and obtain:

$$\frac{d}{dt}\langle\rho(t)\rangle = L_q(t)\langle\rho(t)\rangle + \lambda(t)L_x\langle\xi(t)\rho(t)\rangle \tag{5.28}$$

Now we need to come up with an equation for $\mu(t) = \langle\xi(t)\rho(t)\rangle$. To obtain this equation we multiply the Bloch equation (5.25) by $\xi(t)$ and replace $\langle\xi(t)\dot{\rho}(t)\rangle$ using Shapiro-Loginov formula (5.24). After multiplication by $\xi(t)$ the second term in Eq. (5.25) will be proportional to $\langle\rho(t)\rangle \times$ const because $\xi^2(t) = 1$. This yields

$$\frac{d}{dt}\mu(t) + 2\gamma\mu(t) = L_q(t)\mu(t) + \lambda(t)L_x\langle\rho(t)\rangle \tag{5.29}$$

Therefore we obtained a closed system of linear differential equations which can be expressed compactly in a matrix form as

$$\begin{pmatrix} \dot{\rho}(t) \\ \dot{\mu}(t) \end{pmatrix} = \mathcal{L}(t) \begin{pmatrix} \rho(t) \\ \mu(t) \end{pmatrix} \tag{5.30}$$

where

$$\mathcal{L}(t) = \begin{pmatrix} L_q(t) & \lambda(t)L_x \\ \lambda(t)L_x & L_q(t) - 2\gamma I_q \end{pmatrix} \tag{5.31}$$

is 6×6 matrix comprised of four 3×3 blocks, I_q is a 3×3 unit matrix. The system of linear differential equations (5.30) must be solved with the initial conditions $\mu(0) = \langle\xi(0)\rho(0)\rangle = \langle\xi(0)\rangle\langle\rho(0)\rangle = 0$. From now on we will omit angular brackets for averaged quantities and assume that $\rho(t)$ is the averaged density matrix (like in Eq. (5.30)) unless specified otherwise.

It is seen from this equation that, as mentioned earlier if $\lambda(t)$ has an oscillating component with typical period $T_\lambda \ll \gamma^{-1}, |\lambda|^{-1}$, this component leads to the terms in $\rho(t), \mu(t)$ oscillating with the same period. The amplitude of these terms is $\propto (\gamma T)^{-1}, |\lambda T|^{-1} \ll 1$. This justifies keeping only the time-independent term in λ.

The Liouvillian $\mathcal{L}(t)$ can be expressed in the operator form using Pauli matrices:

$$\mathcal{L}(t) = I_2 \otimes L_q(t) + \lambda\sigma_x \otimes L_x + \gamma\left(\sigma_z - I_2\right) \otimes I_q \tag{5.32}$$

This form will be important for generalization to a multi-fluctuator case. Let us split Liouvillian (5.32) into two parts such that $\mathcal{L} = \mathcal{L}_q + \mathcal{L}_{noise}$, where $\mathcal{L}_q$ is the first term in Eq. (5.32) and $\mathcal{L}_{noise}$ is the sum of the second and third terms. If $\omega(t) = 0$ the matrices $\mathcal{L}_q$ and $\mathcal{L}_{noise}$ commute and can be diagonalized separately.

$$\varrho(t) = e^{\mathcal{L}_q G(t)} e^{\mathcal{L}_{noise} t} \varrho(0) \tag{5.33}$$

$$G(t) = \int_0^t g(\tau) d\tau \tag{5.34}$$

Here $\varrho(t)$ is the generalized density matrix such that $\varrho^T(t) = (\rho(t), \mu(t))$. The Liouvillian $\mathcal{L}_q$ describes uniform rotation of the Bloch vector in yz plane while $\mathcal{L}_{noise}$ describes its dynamics in the corresponding rotating frame. The explicit form of the matrix matrix $\mathcal{L}_{noise}$ is:

$$\mathcal{L}_{noise} = 2 \begin{pmatrix} -\gamma & 0 & 0 & 0 & 0 & 0 \\ 0 & -\gamma & 0 & 0 & 0 & -\lambda \\ 0 & 0 & -\gamma & 0 & \lambda & 0 \\ 0 & 0 & 0 & 0 & 0 & 0 \\ 0 & 0 & -\lambda & 0 & 0 & 0 \\ 0 & \lambda & 0 & 0 & 0 & 0 \end{pmatrix} \tag{5.35}$$

The eigenvalues and eigenvectors of $\mathcal{L}_{noise}$ can be obtained by solving two quadratic equations. As a result, for the initial condition $N(0) = 1$ we obtain:

$$N(t) = \cos(2G(t))\chi(t) \tag{5.36}$$

$$Q(t) = \sin(2G(t))\chi(t) \tag{5.37}$$

$$P(t) = 0 \tag{5.38}$$

where

$$\chi(t) = e^{-\gamma t} \left(\cosh(\Omega t) + \frac{\gamma}{\Omega} \sinh(\Omega t) \right) \tag{5.39}$$

where Ω is as given in Eq. 5.12. As required, this solution is identical to that found using the direct averaging approach.

The solution in the case of CPMG decay is found nearly identically to the Coupler Ramsey solution. It is most convenient to break the evolution into stages. Identically to the previous section, we can use the Shapiro-Loginov equation to find the evolution during g pulses for the generalized density matrix ϱ,

$$\frac{d\varrho}{dt} = (iH_G(t) + L_G)\varrho \tag{5.40}$$

where $H_G(t)$ represents the driving from the coupler and L_G is the coupler noise. These matrices commute, so the solution is given in terms of two commuting propagators,

$$\varrho(t + T_G) = X_G U_G \varrho(t) \tag{5.41}$$

As above, the eigenvectors of $H_G(t)$ are time-independent, so the propagator is found easily. Similarly, the evolution during the frequency pulses is given by,

$$\varrho(t + T_P) = X_P U_P \varrho(t) \tag{5.42}$$

We know that the coupler noise is approximately zero when the coupler is off, so the operator U_P represents the frequency pulse itself and X_P represents the evolution of the uncoupled fluctuator during the pulse. Therefore, we can write the solution after n repetitions of the drive pulse via,

$$\varrho(nT_C) = (X_G U_G X_P U_P X_G U_G)^n \varrho(0) \tag{5.43}$$

In the case where U_P is a π pulse and $T_P \to 0$, the above matrix reduces to a block diagonal form where at most 2 elements are coupled to each other. The evolution of

the z component of the Bloch vector is given by,

$$\frac{d}{dt}\begin{pmatrix}\langle N(t)\rangle\\ \langle\xi(t)P(t)\rangle\end{pmatrix} = (XZX)^n \begin{pmatrix}\langle N(t)\rangle\\ \langle\xi(t)P(t)\rangle\end{pmatrix} \tag{5.44}$$

where $P(t)$ is the x-component of the Bloch vector, and the matrix XZX is identical to the one found in Eq. 5.18. The solution is then also given by Eq. 5.22, as required.

The problem of many fluctuators coupling to a single qubit must also be considered. Before we proceed with this we need to investigate the statistical properties of of a product of many RTN variables $\xi_1(t)\xi_2(t)\ldots\xi_N(t)$. Let us consider a product of two independent telegraph variables $\xi(t) = \xi_1(t)\xi_2(t)$ and find its distribution based on the distributions of $\xi_1(t)$ and $\xi_2(t)$. It is sufficient to concentrate on only one initial condition, e.g. $\xi(0) = +1$. Based on the probability calculus for discrete and independent random variables we can express the probabilities $P^{\xi}_{++}(t)$ and $P^{\xi}_{+-}(t)$ as follows:

$$P^{\xi}_{++}(t) = \frac{1}{2}\left(P^{\xi_1}_{++}(t)P^{\xi_2}_{++}(t) + P^{\xi_1}_{--}(t)P^{\xi_2}_{--}(t) + P^{\xi_1}_{+-}(t)P^{\xi_2}_{+-}(t) + P^{\xi_1}_{-+}(t)P^{\xi_2}_{-+}(t)\right) \tag{5.45}$$

$$P^{\xi}_{+-}(t) = \frac{1}{2}\left(P^{\xi_1}_{++}(t)P^{\xi_2}_{+-}(t) + P^{\xi_1}_{--}(t)P^{\xi_2}_{-+}(t) + P^{\xi_1}_{+-}(t)P^{\xi_2}_{++}(t) + P^{\xi_1}_{-+}(t)P^{\xi_2}_{--}(t)\right), \tag{5.46}$$

where the factor $1/2$ is because there are two equally probable and indistinguishable cases ($\xi_1(0), \xi_2(0) = +1, +1$ and $\xi_1(0), \xi_2(0) = -1, -1$) satisfying initial condition $\xi(0) = +1$, and the distributions functions for individual fluctuators are:

$$P^{\xi_i}_{\sigma_0,\sigma}(t) = \frac{1}{2} + \left(\delta_{\sigma_0,\sigma} - \frac{1}{2}\right)e^{-2\gamma_i t} \tag{5.47}$$

Substitution of Eq. (5.47) into Eqs. (5.45) and (5.46) yields:

$$P^{\xi}_{++}(t) = \frac{1}{2}\left(1 + e^{-2(\gamma_1+\gamma_2)t}\right) \tag{5.48}$$

$$P^{\xi}_{+-}(t) = \frac{1}{2}\left(1 - e^{-2(\gamma_1+\gamma_2)t}\right) \tag{5.49}$$

Eqs. (5.48) and (5.49) ensure that any product of independent telegraph variables is also a telegraph variable with the switching rate $\gamma = \sum_i \gamma_i$. As such, we can apply the Shapiro-Loginov formula to a product of any number of telegraph variables and repeat the procedure described in the previous section.

Now we are ready to describe a set of M fluctuators coupled to our two-qubit system. To understand the structure of the master equations let us imagine that $L_q = 0$ and both L_x and L_q are scalars. We make these assumptions only for instructive purposes because they are nonsensical in the context of Bloch equations. For the sake of simplicity, we assume that $M = 2$. Repeating the single fluctuator procedure described above, i.e. multiplying "master equations" sequentially by $\xi_1(t)$, $\xi_2(t)$, and $\xi_1(t)\xi_2(t)$, using $\xi_i^2(t) = 1$ and applying Shapiro-Loginov formula we obtain:

$$\frac{d}{dt}\begin{pmatrix} \rho \\ \mu_1 \\ \mu_2 \\ \mu_{12} \end{pmatrix} = \begin{pmatrix} 0 & \lambda_2 & \lambda_1 & 0 \\ \lambda_2 & -2\gamma_2 & 0 & \lambda_1 \\ \lambda_1 & 0 & -2\gamma_1 & \lambda_2 \\ 0 & \lambda_1 & \lambda_2 & -2\gamma_1 - 2\gamma_2 \end{pmatrix} \begin{pmatrix} \rho \\ \mu_1 \\ \mu_2 \\ \mu_{12} \end{pmatrix} \tag{5.50}$$

where $\mu_1(t) = \langle \xi_1(t)\rho(t) \rangle$, $\mu_2(t) = \langle \xi_2(t)\rho(t) \rangle$ and $\mu_{12}(t) = \langle \xi_1(t)\xi_2(t)\rho(t) \rangle$. It is straightforward now to rewrite the matrix in Eq. (5.50) in the operator form:

$$\mathcal{L} = \lambda_1 \sigma_x \otimes I_2 + \lambda_2 I_2 \otimes \sigma_x + 2\gamma_1 \sigma_z \otimes I_2 + 2\gamma_2 I_2 \otimes \sigma_z - 2(\gamma_1 + \gamma_2) I_4 \tag{5.51}$$

As such we can associate the matrices $\sigma_\alpha \otimes I_2$ and $I_2 \otimes \sigma_\alpha$ with fluctuators 1 and 2 respectively. Generalization to any number of fluctuators and any qubit Liouvillian is straightforward and we arrive at the following Liouvillian of the system of M fluctuators coupled to a two-qubit system:

$$\mathcal{L} = I_{2^M} \otimes L_q(t) + \sum_{i=1}^{M} \lambda_i \sigma_x(i) \otimes L_x + \sum_{i=1}^{M} \gamma_i \left(\sigma_z(i) - I_{2^M} \right) \otimes I_d, \tag{5.52}$$

where

$$\sigma_\alpha(i) = I_2 \otimes I_2 \otimes \cdots \otimes \sigma_\alpha \otimes \cdots \otimes I_2 \tag{5.53}$$

and the Pauli matrix σ_α is exactly at i_{th} position in this product. Eq. (5.52) can be interpreted as a central spin problem describing the Ising-type interaction of the individual fluctuators (peripheral spins) with the two-qubit system (central spin). In the case $\Delta(t) = 0$ when the qubit Liouvillian commutes with the noise Hamiltonian this problem can be solved exactly.

At first, one needs to transform the equations of motion to a rotating frame associated with g. Then in the absence of the z-component of the magnetic field ($\Delta(t) = 0$) the fluctuators do not interact with each other and eigenvalues of the operator L_x are good quantum numbers. As such, each peripheral spin senses only the local "magnetic field" with x-component 0, or $\pm 4\pi\lambda_i$, imaginary z-component $2i\gamma_i$. Therefore the Liouvillian can be diagonalized by rotating the quantization axis of each spin to a local frame defined by this magnetic field. Since one of the filed components is imaginary this transformation is described by a hyperbolic rotation for each qubit:

$$z_i = \begin{pmatrix} \cosh\left(\frac{\beta_i}{2}\right) & i\sinh\left(\frac{\beta_i}{2}\right) \\ -i\sinh\left(\frac{\beta_i}{2}\right) & \cosh\left(\frac{\beta_i}{2}\right) \end{pmatrix}, \tag{5.54}$$

where

$$\cosh(\beta_i) = \frac{\gamma_i}{\sqrt{\gamma_i^2 - 16\pi^2\lambda_i^2}} \tag{5.55}$$

To diagonalize the Liouvillian (5.52) we construct $2^M \times 2^M$ rotation matrices

$$\zeta(i) = I_2 \otimes I_2 \otimes \cdots \otimes z_i \otimes \cdots \otimes I_2 \tag{5.56}$$

where z_i is at i_{th} position in this product. It is convenient to rewrite Eq. (5.52) as

$$\mathcal{L}_r(t) = L_q(t) \otimes I_{2^M} + L_x \otimes \sum_{i=1}^{M} \lambda_i \sigma_x(i) + I_d \otimes \sum_{i=1}^{M} \gamma_i \left(\sigma_z(i) - I_{2^M}\right), \tag{5.57}$$

which corresponds to the master equation

$$\dot{\varrho}(t) = \varrho(t)\mathcal{L}_r(t) \tag{5.58}$$

Then we diagonalize L_x to separate the blocks corresponding to its eigenvalues $\pm i$ and 0. The transformation, which completely diagonalizes $\mathcal{L}_r(t)$ in the rotating frame takes the form:

$$\mathcal{L}_{diag} = Z^\dagger \mathcal{U}_x^\dagger \mathcal{L}_r \mathcal{U}_x Z, \tag{5.59}$$

where

$$Z = (P_+ + P_-) \otimes \prod_{i=1}^{M} \zeta(i) + P_0 \otimes I_{2^M}, \tag{5.60}$$

$P_\pm$ and P_0 are the projectors onto the eigenstates of L_x with eigenvalues $\pm i$ and 0, respectively, $\mathcal{U}_x = u_x \otimes I_{2^M}$ and

$$u_x = \begin{pmatrix} 0 & 0 & 1 \\ -\frac{i}{\sqrt{2}} & \frac{i}{\sqrt{2}} & 0 \\ \frac{1}{\sqrt{2}} & \frac{1}{\sqrt{2}} & 0 \end{pmatrix} \tag{5.61}$$

is the matrix diagonalizing L_x. After this transformation, the problem is reduced to solving 3×2^M linear differential equations, and the final result corresponding to the initial condition $N(0) = 1$ reads:

$$N(t) = \cos(2G(t))\chi(t) \tag{5.62}$$

$$Q(t) = \sin(2G(t))\chi(t) \tag{5.63}$$

$$P(t) = 0 \tag{5.64}$$

where

$$\chi(t) = \prod_k e^{-\gamma_k t} \left(\cosh(\Omega_k t) + \frac{\gamma_k}{\Omega_k} \sinh(\Omega_k t) \right) \tag{5.65}$$

In real experiments, there is noise present other than the coupler noise we are focused on. For example, independent single qubit decay and dephasing may contribute significantly to what is seen in experimental measurements. Single qubit decay and

dephasing can be modeled alongside classical coupler noise via the Lindblad equation,

$$\begin{aligned}\frac{d\rho}{dt} =& -i[H(t),\rho] + L_t[\rho] + L_l[\rho] \\ L_t[\rho] =& \sum_{m=1}^{2} \Gamma_m^{\phi} \left(n_m n_m \rho(t) - \frac{1}{2}\{n_m n_m, \rho(t)\} \right) \\ L_l[\rho] =& \sum_{m=1}^{2} \Gamma_m^{1} \left(\sigma_m^- \rho(t) \sigma_m^+ - \frac{1}{2}\{\rho(t), \sigma_m^+ \sigma_m^-\} \right)\end{aligned} \tag{5.66}$$

where n_m is the number operator for qubit m and σ_m^- and σ_m^+ are the annihilation and creation operators for qubit m, respectively. First, we will focus on the free evolution problem. It is most convenient to divide the total Hamiltonian (3.4) into two parts,

$$\begin{aligned}H(t) =& H_C(t) + H_N(t) \\ H_C(t) =& g(t)\sigma_x \\ H_N(t) =& \lambda(t)\xi(t)\sigma_x\end{aligned} \tag{5.67}$$

Let $U_C(t)$ be the unitary generated by H_C.

$$\begin{aligned}U_C(t) =& e^{-i\sigma_x G(t)} \\ G(t) =& \int_0^t g(\tau) d\tau\end{aligned} \tag{5.68}$$

Eq. 5.66 can then be moved into the interaction picture of $U_C(t)$. Defining $\tilde{\rho} = U_C^{\dagger} \rho U_C$ and noting that $[U_C, H_N] = 0$,

$$\begin{aligned}\frac{d\tilde{\rho}}{dt} =& -i[H_N(t),\tilde{\rho}] + \tilde{L}_t[\tilde{\rho}] + \tilde{L}_l[\tilde{\rho}] \\ \tilde{L}_t[\tilde{\rho}] =& \sum_{m=1}^{2} \Gamma_m^{\phi} \left(\tilde{n}_m \tilde{n}_m \tilde{\rho} - \frac{1}{2}\{\tilde{n}_m \tilde{n}_m, \tilde{\rho}\} \right) \\ \tilde{L}_l[\tilde{\rho}] =& \sum_{m=1}^{2} \Gamma_m^{1} \left(\tilde{\sigma}_m^- \tilde{\rho} \tilde{\sigma}_m^+ - \frac{1}{2}\{\tilde{\rho}, \tilde{\sigma}_m^+ \tilde{\sigma}_m^-\} \right)\end{aligned} \tag{5.69}$$

where the notation $\tilde{a} = U_C^\dagger a U_C$ is used for the jump operators. If this equation is expanded in the vectorized σ_x basis , $\tilde{\rho} = \Big(\langle +|\tilde{\rho}|+\rangle, \langle +|\tilde{\rho}|-\rangle, \langle -|\tilde{\rho}|+\rangle, \langle -|\tilde{\rho}|-\rangle\Big)^T$,

$$\frac{d\tilde{\rho}}{dt} = \mathcal{L}_{\text{lind}}(t)\tilde{\rho} \tag{5.70}$$

$$\mathcal{L}_{\text{lind}}(t) = \frac{1}{4}\begin{pmatrix} (-\Gamma_\phi - 2\Gamma_1) & \Delta\Gamma_1 e^{-2iG(t)} & \Delta\Gamma_1 e^{2iG(t)} & \Gamma_\phi \\ \Delta\Gamma_1 e^{2iG(t)} & (-8i\xi(t)\lambda(t) - \Gamma_\phi - 2\Gamma_1) & e^{4iG(t)}\Gamma_\phi & \Delta\Gamma_1 e^{2iG(t)} \\ \Delta\Gamma_1 e^{-2iG(t)} & e^{-4iG(t)}\Gamma_\phi & (8i\xi(t)\lambda(t) - \Gamma_\phi - 2\Gamma_1) & \Delta\Gamma_1 e^{-2iG(t)} \\ \Gamma_\phi & \Delta\Gamma_1 e^{-2iG(t)} & \Delta\Gamma_1 e^{2iG(t)} & (-\Gamma_\phi - 2\Gamma_1) \end{pmatrix} \tag{5.71}$$

where $\Gamma_1 = \Gamma_1^1 + \Gamma_2^1$, $\Delta\Gamma_1 = \Gamma_2^1 - \Gamma_1^1$, and $\Gamma_\phi = \Gamma_1^\phi + \Gamma_2^\phi$. Note that this equation will yield the solution for a single trajectory of $\xi(t)$, since $\xi(t)$ is a random process.

Several simplifications can be made to this equation. First of all, if the driving is periodic, then $\lambda(t)$ may be replaced with its average value, as justified previously. The time dependence of $G(t)$ can be handled in several ways. Depending on the applied control, it may be justified to assume $g(t)$ is a constant g, in which case $G(t) \to gt$. This is useful because it would allow for analytical solution of the averaged equations. Here, we have a different physical limit that allows even further simplification. In our experiments, $g(t)$ is generally on the order of 10MHz, while λ, γ and Γ are generally less than 1 MHz. Therefore, these quickly rotating terms can be dropped which yields a set of ODEs for $\tilde{\rho}$ in which the only time dependence in the coefficients comes from $\xi(t)$.

Next $\tilde{\rho}$ must be averaged over $\xi(t)$. This can be done using the Shapiro-Loginov equation. We can arrive at a set of constant coefficient linear ODEs for the averaged $\tilde{\rho}$ and μ (as defined near Eq. 5.28),

$$\begin{pmatrix} \dot{\tilde{\rho}} \\ \dot{\mu} \end{pmatrix} = \mathcal{L}_{SL} \begin{pmatrix} \tilde{\rho} \\ \mu \end{pmatrix} \tag{5.72}$$

If $\tilde{\rho}$ is given in the vectorized energy basis,

$$\tilde{\rho} = \Big(\langle 01|\tilde{\rho}|01\rangle, \langle 01|\tilde{\rho}|10\rangle, \langle 10|\tilde{\rho}|01\rangle, \langle 10|\tilde{\rho}|10\rangle\Big)^T \tag{5.73}$$

$\mathcal{L}$ is given by,

$$\mathcal{L}_{SL} = \begin{pmatrix} A & B \\ B & A - \gamma I \end{pmatrix} \tag{5.74}$$

$$A = \frac{1}{8}\begin{pmatrix} -4\Gamma_1 - \Gamma_\phi & 0 & 0 & \Gamma_\phi \\ 0 & -4\Gamma_1 - 3\Gamma_\phi & -\Gamma_\phi & 0 \\ 0 & -\Gamma_\phi & -4\Gamma_1 - 3\Gamma_\phi & 0 \\ \Gamma_\phi & 0 & 0 & -4\Gamma_1 - \Gamma_\phi \end{pmatrix} \tag{5.75}$$

$$B = i\lambda \begin{pmatrix} 0 & 1 & -1 & 0 \\ 1 & 0 & 0 & -1 \\ -1 & 0 & 0 & 1 \\ 0 & -1 & 1 & 0 \end{pmatrix} \tag{5.76}$$

$\mathcal{L}_{SL}$ is analytically diagonalizable, so the dynamics can easily be computed in closed form. Particularly relevant to experiments is the normalized $\langle \sigma_z \rangle$ observable,

$$\begin{aligned} \frac{\langle 01|\tilde{\rho}|01\rangle - \langle 10|\tilde{\rho}|10\rangle}{\langle 01|\tilde{\rho}|01\rangle + \langle 10|\tilde{\rho}|10\rangle} =& e^{-\frac{1}{4}t(4\gamma+\Gamma_\phi)}\left(\cosh(t\Omega) + \frac{\gamma \sinh(t\Omega)}{\Omega}\right) \\ \Omega =& \sqrt{\gamma^2 - 4\lambda^2} \end{aligned} \tag{5.77}$$

Note that this is simply the solution without including white noise (Eq. 5.10) with an additional exponentially decaying prefactor.

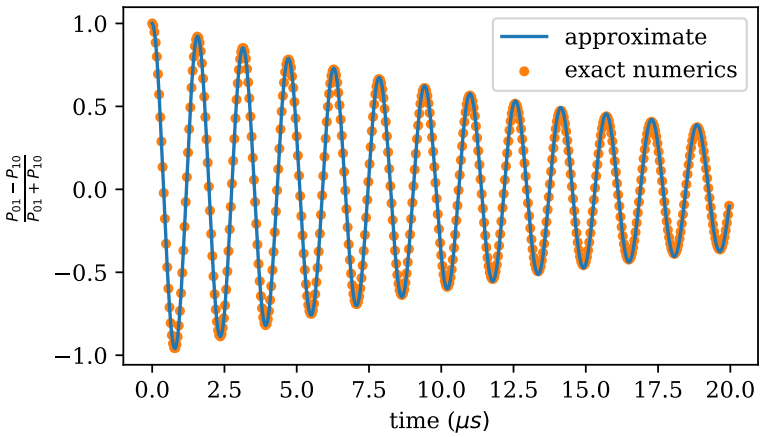

Figure 5-1: Comparison of the approximate solution for the decay envelope of the normalized $\langle\sigma_z\rangle$ in the case of free decay (Eq. 5.77) to exact numerical simulation of the time dependant master equation constructed using eq. 5.70. $g(t)$ was taken to be a 40ns smoothed trapezoidal pulse with a maximum of g_{max}. Parameter values used here are $\gamma = 0.05$MHz, $\lambda = 0.3$MHz, $g_{max} = 10$MHz, $\Gamma_\phi = 0.1$MHz, $\Gamma_1 = 0.15$MHz, and $\Delta\Gamma_1 = 0.05$MHz. This represents the strongest noise we ever see experimentally at an artificially lowered g value, which should be a good stress test for the approximation. The approximation seems to work well over a wide range of parameter values. The envelope function oscillates because these parameter values lead to an under-damped solution.

The solution for CPMG pulse sequences can be found using the free decay solution. In line with the previous section, if the qubit frequency pulses are instantaneous the effective Hamiltonian could be written $H(t) = h(t)(H_C(t) + H_N(t))$, where $h(t)$ is the filter function defined in Eq. 3.13. In this case, the dynamics for a CPMG sequence of a given length would be given by

$$\begin{pmatrix} \dot{\tilde{\rho}} \\ \dot{\mu} \end{pmatrix} = \ldots \mathcal{L}_{\text{even}}\mathcal{L}_{\text{odd}}\mathcal{L}_{\text{odd}}\mathcal{L}_{\text{even}} \begin{pmatrix} \tilde{\rho} \\ \mu \end{pmatrix} \tag{5.78}$$

where $\mathcal{L}_{\text{even}} = \mathcal{L}(\lambda = \lambda)$ and $\mathcal{L}_{\text{odd}} = \mathcal{L}(\lambda = -\lambda)$

If we compute the normalized $\langle\sigma_z\rangle$ observable (as in Eq. 5.11) using this scheme,

we find that it is equivalent to Eq. 5.22 with a prefactor of $e^{-\frac{\Gamma_\phi t}{4}}$.

5.4 Echoing Strongly Coupled Fluctuators

There is an interesting qualitative difference between the results for Gaussian $1/f$ noise (4.29) and a single non-Gaussian RTN fluctuator (5.22). Namely, in the case of the former, it is clear that decay is monotonically suppressed as the number of CPMG pulses in a given time is increased. i.e., the more the noise is echoed the less it affects the qubit system. However, in the case of the latter, it is not at all clear that this happens.

Consider a single, far underdamped fluctuator, $\lambda >> \gamma$. Then,

$$\Omega = i\overline{\omega} \tag{5.79}$$

where $\overline{\omega} = \sqrt{4\lambda^2 - \gamma^2} \approx 2\lambda$ is a real number. If we then make the substitution $\frac{\gamma}{\overline{\omega}} = \epsilon$, equation 5.22 reduces to,

$$\chi(nT_C) \cong e^{-nT_C\gamma} e^{n\epsilon \sin(T_C\overline{\omega})} \tag{5.80}$$

If $n\epsilon << 1$, we can expand to leading order in $n\epsilon \sin\left(\frac{t\omega}{n}\right)$,

$$\chi(nT_C) \cong e^{-nT_C\gamma} \left(1 + n\epsilon \sin(T_C\overline{\omega})\right) \tag{5.81}$$

This equation implies that for modest n, increasing the number of echoing pulses will not protect qubits from the dephasing effects of the strongly coupled fluctuator given that we keep $t = nT_C$ constant. Only when $n\epsilon > 1$ do we start to see significant protection from the noise. This is shown in figure 5-2. This behavior is qualitatively quite different from what happens with Gaussian $1/f$-type noise, where increasing the number of echo pulses that occur in time t will move the center of the filter function to higher frequencies and monotonically reduce dephasing.

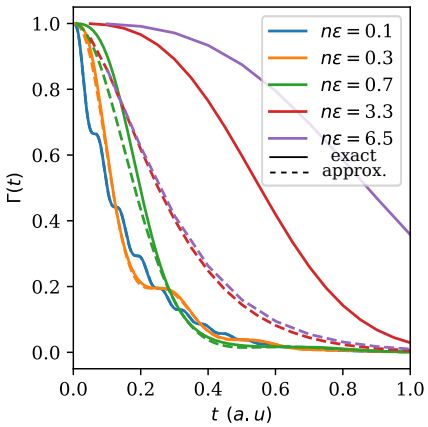

Figure 5-2: Comparing exact and analytical solutions for the echoed decay envelope. Exact solutions are calculated using Eq. 5.22 and are shown in solid lines, while the approximate solutions are calculated using Eq. 5.81 and are shown by dashed lines. The approximation is almost exact for the two lowest values of $n\epsilon$, but has significant error for $n\epsilon > 1$.

Chapter 6

Experimental Characterization of g-Noise

The work reported so far in this thesis constitutes the design of an experiment for characterizing g-noise and a detailed analysis of what measurement results would be expected under a few plausible noise models. In this section, we will proceed with running and evaluating the results of our experiment on a tunable-Transmon architecture superconducting quantum computer.

We evaluate measured coupler Ramsey and CPMG signals against Gaussian noise models of chapter 4, and find that they do not explain several features seen in the data, namely stepping in the CPMG envelopes. We then demonstrate that these steps are well explained by the RTN models of section 5. Via independent experiments and theoretical analysis, we argue that these steps are genuine evidence of RTN noise in the coupler, and are not simple experimental artifacts. This is a significant finding: clean examples of non-Gaussian fluctuations in qubit experiments are rare.

We begin by outlining some details of our experiment in section 6.1. Sections 6.2, 6.3, and 6.4 compare experimental measurements to the Gaussian and non-Gaussian models produced in previous chapters, and conclude that our device indeed experiences noise during two-qubit gates that is not well-described by a Gaussian model. In sections 6.5 and 6.6 we further support this conclusion by theoretically studying the effect of pulse errors on our experiments and by doing an entirely independent

experiment using a different control scheme that independently verifies our conclusion.

6.1 Experimental Protocol and Calibration

Our experiments were run on a Sycamore class quantum processor, as used in the quantum supremacy experiment [31]. The basic bring up and calibration of these kinds of devices, such as establishing readout and single-qubit gate functionality, is carried out by an automated tool called Optimus [81].

As described in chapter 3, our experiment involves applying many sequential two-qubit gates. As such, ensuring the fidelity of these operations is critical, as errors may accumulate and ruin our measured signal. To do this, we used a Heisenberg-limited metrology technique called floquet calibration that has been experimentally proven to be able to identify the parameters of the iSWAP-like gates to a precision of $\sim 10^{-4}$ rad [25, 26]. The method is outlined in detail in both of these works; the basic idea is that by repeating an operation N times in a way that errors accumulate coherently, the precision with which systematic errors can be measured scales as $1/N$, instead of standard $1/\sqrt{N}$ shot noise scaling. The use of this technique in a closed-loop calibration of the gate parameters allows us to be quite confident that we are implementing the operations we think we are.

Another important aspect of our experimental technique is post-selection. We measure a scaled σ_z observable,

$$\frac{\langle \sigma_z \rangle}{\langle I \rangle} = \frac{\langle 01|\rho(t)|01\rangle - \langle 10|\rho(t)|10\rangle}{\langle 01|\rho(t)|01\rangle + \langle 10|\rho(t)|10\rangle} , \tag{6.1}$$

This normalization of $\langle \sigma_z \rangle$ eliminates the effect of T_1 noise in relevant cases, see chapter 5. The simple intuition behind this is that T1 is the only process that can take the state of our system out of the single excitation subspace, and once it leaves it cannot come back. Therefore, by scaling our measurements by the total population that remains in the single excitation subspace, we reverse the effect of T1.

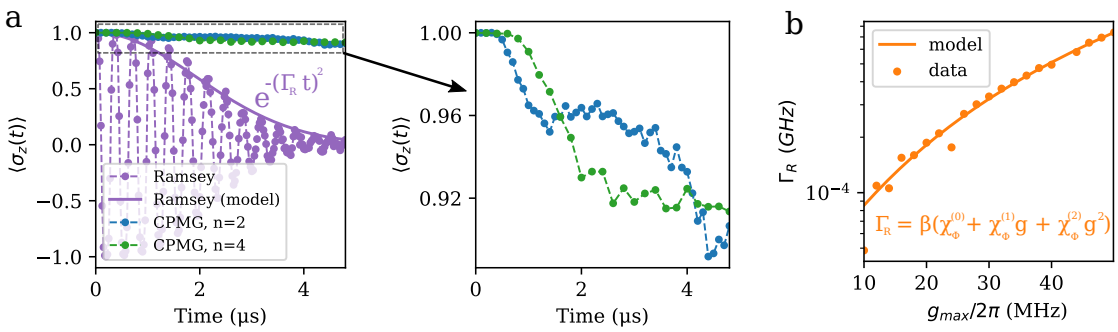

Figure 6-1: **Experimentally observed Ramsey and CPMG dynamics. (a)** Comparing Coupler Ramsey decay of normalized population difference (Eq. 6.1) with $g_{max} = 30$MHz to decay under $n = 2$ and $n = 4$ Coupler CPMG sequences. The x-axis is total evolution time, $t = nt_g$ for Ramsey and $t = 2mnt_g$ for CPMG. The duration of a fixed n CPMG sequence is modified by changing m. We see that the CMPG sequences effectively mitigate most of the decoherence, suggesting that most of the noise power is at low frequencies. The Gaussian shape of the Ramsey decay envelope is typical of 1/f-type noise (see Eq. 4.12). When observed in detail, the CPMG decay envelopes display behavior not predicted by Gaussian theory. Increasing the number of CPMG pulses does not increase noise protection as predicted by Eq. 4.29; the curves braid and have steps. All data points are the average of 10000 samples. **(b)** Ramsey decay rate Γ_R vs $g_{\max}$. We see that the decay rate is strongly dependent on $g_{\max}$, crossing an order of magnitude in 30 MHz. The $g_{\max}$-dependence is well-predicted by Eq. 2.8 given typical circuit parameters.

6.2 Experimental Results vs Gaussian Theory

Our first set of experiments set out to test the basic predictions of our physical model of coupler flux noise (see chapter 2) and our Gaussian noise model (see section 4) against measurements from our device. We perform measurements for many different values of the qubit-qubit coupling g and different numbers of CPMG pulses n, including $n = 0$ (Ramsey). The results are summarized in Fig. 6-1.

The purple curve in the left panel of Fig. 6-1 (a) compares the measured Ramsey decay envelope against the form predicted by a Gaussian $1/f$ noise model (Eq. 4.12). The experimentally measured decay envelope seems to be well predicted by Gaussian $1/f$ noise. We may also compare how the envelope changes with g with what would be predicted by our physical model of coupler flux sensitivity (Eq. 2.8). We can extract a measured flux sensitivity function by recording the measured Ramsey decay rate

Γ_R vs g. We can then fit the measured sensitivity function to a quadratic model of the form of our expansion Eq. 2.8. We are most interested in the ratio between the quadratic and linear components, $\chi_\Phi^{(2)}/\chi_\Phi^{(1)}$, as the constant term does not scale with g and therefore may easily be influenced by other experimental imperfections. From the data we extract a value of $\chi_\Phi^{(2)}/\chi_\Phi^{(1)} \approxeq 0.078$ ns, while a purely theoretical calculation using typical circuit parameters yields $\chi_\Phi^{(2)}/\chi_\Phi^{(1)} \approxeq 0.08$ ns. This excellent agreement with theory strongly suggests that noise during two-qubit gates is dominated by flux noise in the coupler, as hypothesized.

As shown in the left panel of Fig. 6-1 (a), the CPMG envelopes decay significantly slower than the Ramsey envelopes. As discussed in chapter 4, this agrees with the Gaussian theory. However, as shown in Fig. 6-1 the details of these curves deviate from what would be predicted by Gaussian $1/f$ noise. While Eq. 4.29 predicts smooth decay, we see very clear steps in the decay curves. Additionally, the model predicts that the decay rate Γ_C should decrease proportionately to $\frac{1}{\sqrt{n}}$. This is not seen at all: the two curves "braid" and decay at the same rate. As argued at the end of chapter 4, this is likely a signature of non-Gaussian contributions to the noise.

6.3 Experimental Signatures of Telegraph Noise

We then set out to carefully test our models of RTN g-noise, and see if they could explain the steps visible in our data. To minimize the effects of various experimental drifts, we selected a few values of g and n and rapidly completed CPMG measurements back to back. We then attempted to simultaneously fit each data set to the three-parameter single RTN model (γ, λ, and Γ_ϕ, see Eq. 5.22).

The results of the measurements and the fitting procedure are shown in Fig. 6-2. The decay envelopes are excellently described by a single, under-damped RTN fluctuator alongside single qubit white noise dephasing, which adds a simple exponential prefactor $e^{-\frac{\Gamma_\phi}{4}t}$ to Eq. (5.22), see chapter 5.

To push our model even further, we then attempted to simultaneously fit CPMG data collected for 5 different values of n and a single value of g. The results of this

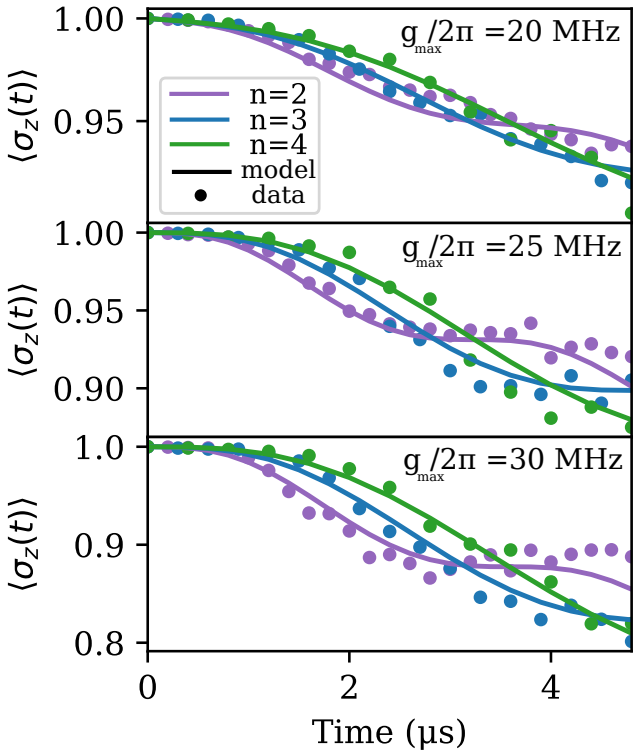

Figure 6-2: **Braiding in the CPMG decay envelopes** Fitting a single-fluctuator model to CPMG decay envelopes (Eq. 5.22) for different values of n and g_{max}. Each set of 3 curves is fit using only 3 parameters, γ, λ, and Γ_ϕ. Fits for more values of n can be found in supplementary material section I. Typical values of $t_c = \frac{1}{\gamma} \approxeq 50\mu$s, $\frac{\lambda}{2\pi} \approxeq 0.1 - 1$MHz (value depends strongly on g), and $\Gamma_\phi^{-1} \approxeq 100\mu s$. All data points are the average of 10000 samples.

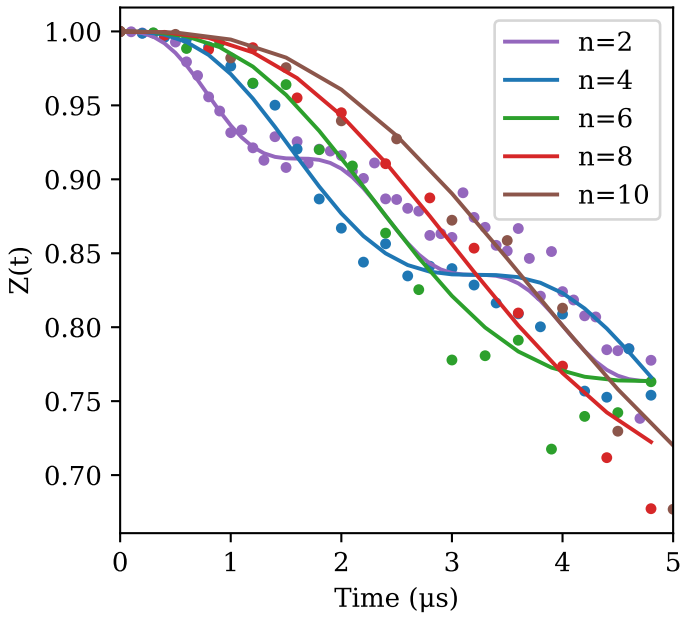

Figure 6-3: Fit of the 3 parameter single fluctuator model to 5 CPMG curves simultaneously. As standard, the x-axis is real-time, $t = 2mnt_g$. m is varied to change the duration of a constant n CPMG sequence.

are shown in Fig. 6-3

The 5-curve data is simultaneously fit well by the single fluctuator model, lending more evidence to the theory of RTN coupler noise.

6.4 Measurement of the Coupling to a Single Fluctuator

The measurements of the previous sections do not attempt to validate that the scaling of the amplitude of a single RTN fluctuator, λ, scales with g following our flux noise theory (chapter 2). In this section, we show the results of experiments that rectify this.

The scaling of λ of a single fluctuator with g can be established by taking CPMG data on the same pair of qubits over a range of values of $g_{\max}$. Fig. 6-4 shows the results of such an experiment.

The data can fit well with a model that includes one slow, strongly coupled fluctuator, white flux noise (emulated by a fast fluctuator), and single-qubit dephasing. The inclusion of white flux noise was critical to achieving a good fit, which is physically reasonable, as echo sequences do not suppress this kind of noise at all. The slow fluctuator has a correlation time of approximately $70\mu s$. This is the strongly coupled, under-damped fluctuator that creates the steps seen in the data and the fit. The single-qubit dephasing rate represents white noise that does not scale with g, and the extracted value of $\frac{1}{\Gamma_\phi} \approxeq 90\mu s$ is reasonable for this device. Ratio $\chi_\Phi^{(2)}/\chi_\Phi^{(1)} \approxeq 0.12$ ns for this data, which is also within expectation.

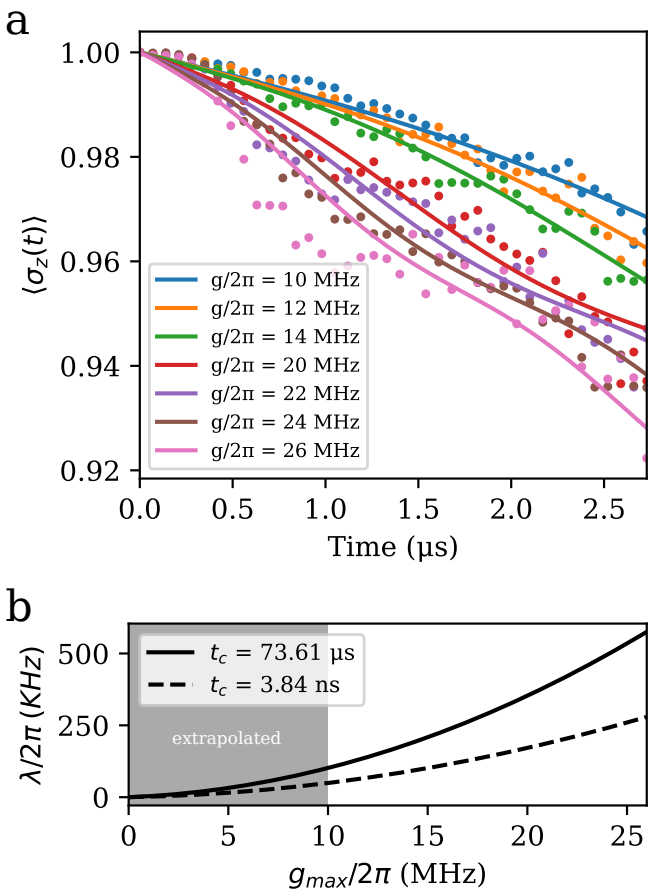

Figure 6-4: **Extracting the scaling of telegraph noise amplitude. a)** Experimental data (dots) vs fit model (lines) for $n = 1$ CPMG sequences at various values of $g_{\max}$. The fit value of T_ϕ is approximately 90 μs, which is a reasonable result for this device. **b)** The extracted noise amplitude $\lambda(g)$ for the two fluctuators. Note that the same function χ_Φ was used for both fluctuators; the g-noise amplitudes were only allowed to differ by an overall scale.

6.5 Effects of Pulse Errors on CPMG

It is reasonable to postulate that the steps in our data observed in the last few sections may not be caused by non-Gaussian fluctuators as we claim, but rather by errors in our pulses. Here we investigate this hypothesis and find that it cannot be true.

In particular, we investigate a possible error in the Z_π-phase gate, which is used

in echo and CPMG sequences. Assuming that our Z-pulses correspond to angle $\pi - \delta$, where δ is the phase error in radians, 5.22 can be easily generalized, and in the case of a single echo pulse ($n = 1$) it assumes a very simple form:

$$\langle \sigma_{z\delta}(t) \rangle = \cos^2\left(\frac{\delta}{2}\right) \langle \sigma_z(t) \rangle + \sin^2\left(\frac{\delta}{2}\right) \cos(2gt) \left(\langle \sigma_z(t) \rangle - \frac{8\lambda^2 e^{-\gamma t} \sinh^2\left(\frac{1}{2}t\sqrt{\gamma^2 - 4\lambda^2}\right)}{\gamma^2 - 4\lambda^2} \right). \tag{6.2}$$

Here $t = 2mt_g$ and $\langle \sigma_z(t) \rangle$ is given by Eq. 5.22 with $n = 1$. As can be seen from Eq. (6.2), the phase error δ gives rise to a high-frequency oscillating term proportional to $\cos(2gt)$. A corresponding shape of the echo signal for a single telegraph fluctuator is shown in Fig. 6-5. As expected, the high-frequency oscillations of the signal are seen but the step-like shape remains robust even for large $\delta \sim 0.3$ radians. For higher CPMG orders the formulas with imprecise Z_π pulse become cumbersome but still can be analyzed and computed straightforwardly. In practice, the phase error can

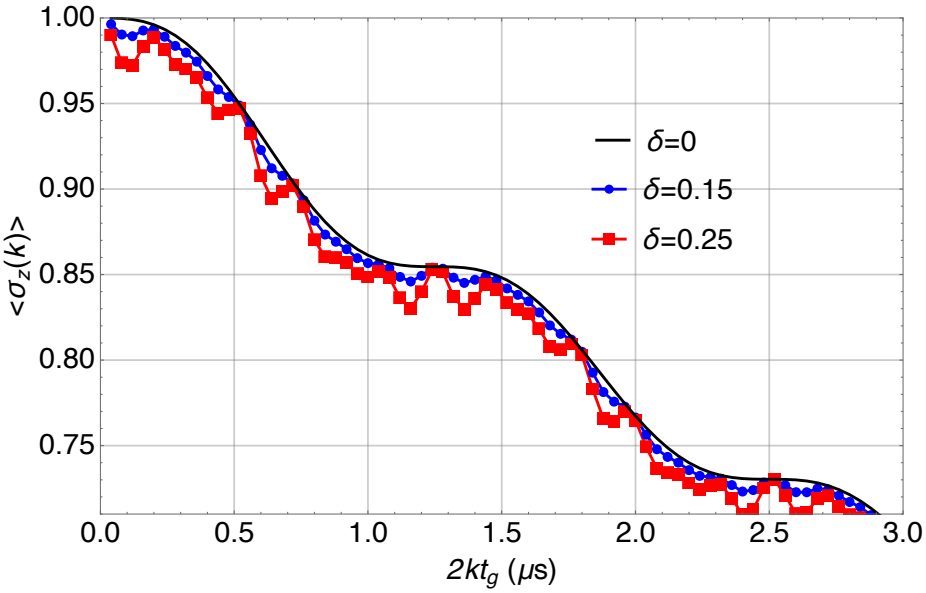

Figure 6-5: Echo RTN signals for different values of the phase error δ

be easily calibrated out by taking a series of 2D scans (see Fig. 6-6) until the fringes corresponding to the erroneous phase gates fade away and completely disappear.

It is also worth discussing our technique and results in the context of the standard

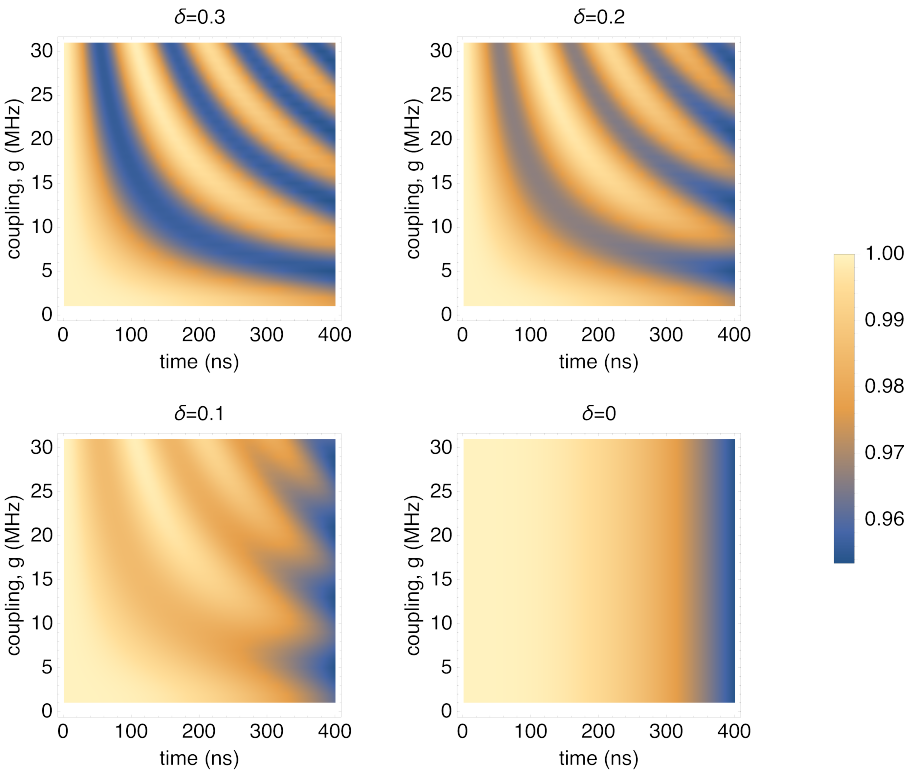

Figure 6-6: 2D-scans used for Z-phase calibration

NMR techniques and nomenclature. There are two major nomenclature and notational differences. First of all, in our case, the axis of 180-degree rotation, which we will call the echo axis, is pointed along z and the static (inhomogeneous or, more precisely, fluctuating) magnetic field is in x direction, $h_x = 2(g + \lambda\xi)$. On the contrary, in the standard NMR nomenclature the echo axis is pointed along x (H_1-field in Ref. [82]), and the static magnetic field is along z-axis. Second, in our case, the first 90-degree pulse is absent because under our technique the two-qubit system is naturally initialized in the state $|10\rangle$, i.e., the initial position of the Bloch vector is along the echo axis. The geometry described above is precisely equivalent to the geometry of the Meiboom-Gill modification of the CPMG method [82]. Indeed, in our case, the (pseudo) Bloch vector undergoes Larmor precession around the static magnetic field, which is parallel to x. In other words, it is rotating around the x axis within the $y-z$ plane starting from $+z$, and all 180-degree echo rotations are performed around the same $+z$ axis. As such, if there is an error in a Z_π pulse and the Bloch vector ends up out of the yz-plane, the next pulse (either under- or over-rotation) will return the Bloch vector to the yz-plane. This non-accumulation of the Z_π error is demonstrated in Fig. 6-7 where we compare the RTN CPMG signals with $\delta = 0.15$ for different orders n of CPMG sequences.

A similar error may arise when there is an uncontrolled static detuning of the qubit frequencies $\delta\omega \ll g$. For example, in the case of the underdamped RTN regime, which is of our primary interest, the correction to Eq. **??** reads:

$$\delta\langle\sigma_z(n\tau_m)\rangle = \begin{cases} -\frac{\delta\omega^2}{g^2} e^{-\gamma n\tau_m} \left(\sin^4\left(\frac{(g+\lambda)\tau_m}{2}\right) + \sin^4\left(\frac{(g-\lambda)\tau_m}{2}\right)\right) + O\left(\frac{\delta\omega^4}{g^4}\right), & n \text{ odd} \\ -O\left(\frac{\delta\omega^4}{g^4}\right), & n \text{ even} \end{cases} \tag{6.3}$$

where $\tau_m = 2mt_g$ is the time interval between neighboring Z_π pulses. We see that the error is small and does not accumulate when we increase the number of CPMG Z_π pulses.

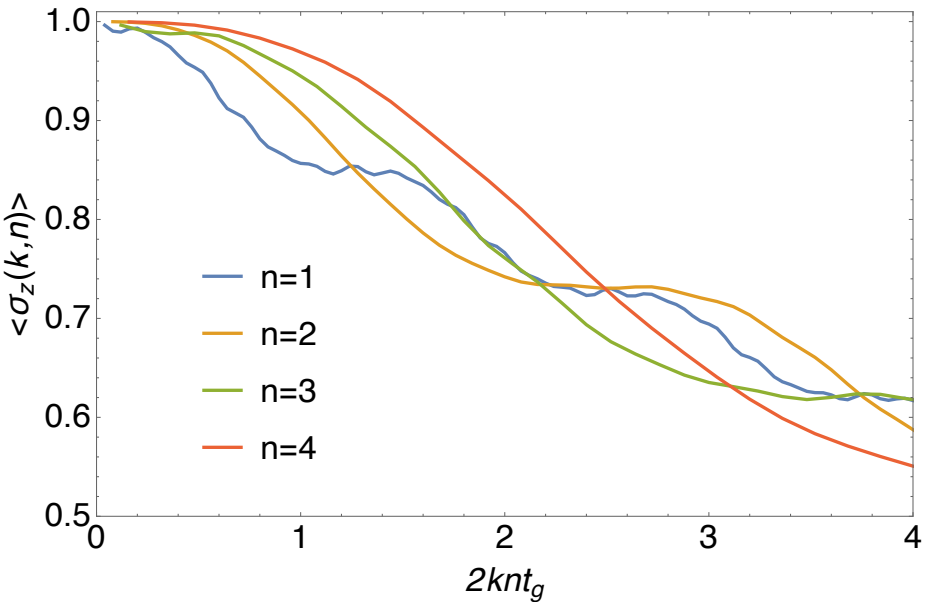

Figure 6-7: CPMG RTN signals for sequences with $n = 1, \ldots 4$ and the Z_π phase error $\delta = 0.15$

6.6 Rebirth of Rabi Oscillations in Ramsey Measurements

To provide evidence of RTN fluctuators that does not rely on the CPMG pulse sequence, we investigated another phenomenon predicted by this model. Namely, in the case of coupler Ramsey decay, the under-damped regime 5.39 predicts that the decay envelope will oscillate. If the coupling to the RTN source is sufficiently strong for the oscillation period to be short compared to the decay induced by quasi-static noise, this oscillation can lead to a "rebirth" of Rabi oscillations.

This rebirth is regularly observed in experimental data. Fig. 6-8 shows two independent examples, taken at different times on different qubits. The left figure shows data taken using the usual pulse-based coupler Ramsey scheme. The right figure shows data taken using a continuous waveform scheme, in which the coupler is turned on at the start of the experiment and left on for the duration, such that g is constant. Both datasets show the rebirth, further supporting the conclusion that the device couples strongly to RTN fluctuators.

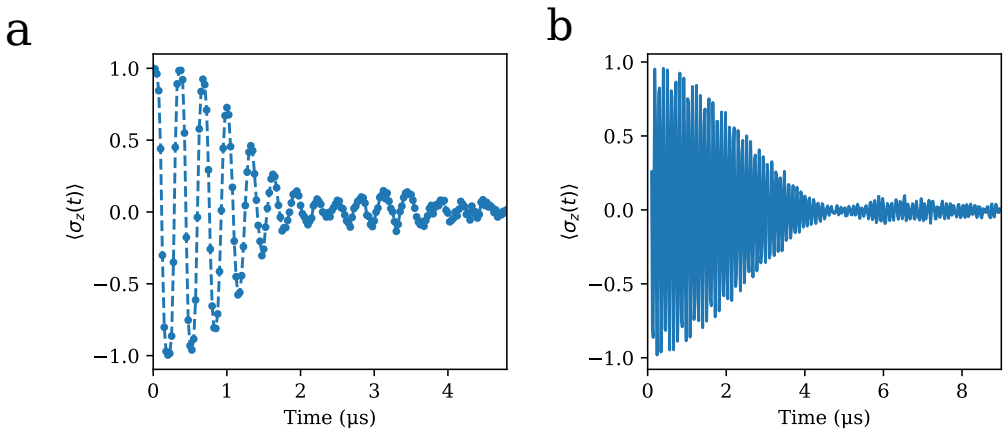

Figure 6-8: Rebirth of Rabi oscillations in **a** pulse-based and **b** continuous waveform coupler Ramsey.

Chapter 7

Conclusions

This thesis constitutes a large body of theoretical and experimental work concerning non-Gaussian flux noise that affects two-qubit gates in the tunable coupler Transmon superconducting qubit architecture. The main conclusion is that this noise is a result of coupler flux fluctuations, which can be dominantly non-Gaussian. This is rigorously backed up by several experimental and theoretical observations:

1. Scaling of the decay rate in a Ramsey experiment that is consistent with coupler flux noise dominating qubit flux noise during gates

2. Stepwise decay in CPMG signals, which cannot be easily produced by any Gaussian model but is the expected result of non- Gaussian RTN

3. Braiding in CPMG signals as the number of CPMG pulses is varied, which is exactly what is predicted by an RTN model

4. Rebirth of Rabi oscillations in both gate-based and continuous waveform Ramsey experiments, a prediction of an RTN model that is independent of any complex pulse sequences that may introduce experimental error

It should be noted that this work alone is not enough to understand the physical origins of this non-Gaussian contribution to the noise in our superconducting system. Although this noise has been observed on several qubits in our system, this has not

been studied systematically enough to determine if different qubits see fluctuators with similar parameters. Additionally, it would be impossible to tell if multiple pairs of qubits are seeing the same physical defect or just similar, independent defects with this kind of time-averaged, two-qubit measurement. These two situations may be discernible using time-averaged measurements taken after periodic pulse sequences on more than two qubits.

While the majority of this work was focused on the details of applying our technique to tunable-coupler transmons, the basic methods transfer readily to other qubit architectures. As an example from trapped ion quantum computing, a similar technique could be used in the characterization of the effect of noise [83] on the coupling developed between ion electronic states during Mølmer-Sørensen gates [84].

This work has elucidated the importance of studying noise via the physics of a specific device, especially as larger and larger quantum computers are built. Indeed, this approach is what allowed us to discover the dominant source of low-frequency noise that occurs during our two-qubit gates. Additionally, we have found very clear signatures of non-Gaussian, non-1/f noise in our solid-state device, which is quite atypical in the field. Further study of this kind of noise may reveal its physical origins, and yield insight into better design, fabrication, or control of quantum devices.

In addition to our contributions to the engineering of quantum computers, we have also unambiguously established that it is possible to build a device that couples strongly to non-Gaussian fluctuations in a controllable and well-characterized manner. This opens the door to building engineered devices that harness natural noise for their benefit in the same way that living things do.

For example, as mentioned in the introduction, non-Gaussian noise leads to exponentially faster escape from potential wells than non-Gaussian noise [21]. It is therefore reasonable to suggest that non-Gaussian noise may be key to accelerating sampling from complicated probability distributions, such as energy-based models [85]. A popular way to perform this sampling currently is the Metropolis-adjusted Langevin algorithm, which uses Eq. 1.2 along with Metropolis-Hastings rejection steps to sample from Gibbs distributions [86]. Deep potential wells slow this algorithm down

by trapping particles in particular regions of state space, prolonging mixing times. Could using a non-Gaussian Langevin equation improve performance? In particular, since we have uncovered a completely physical and analog source of non-Gaussian fluctuations, it may be possible to build a physical device that has short equilibration timescales that still generates samples from a complex distribution. Such a device would essentially be a physics-based accelerator for energy-based models, and could drastically improve the practicality of these modeling techniques.

It is also interesting to think about the role of non-Gaussian noise in machine learning more broadly. Noise is critical to generative modeling broadly, and diffusion models operate on a principle similar to Langevin dynamics [87]. There is some empirical evidence that non-Gaussian diffusion models perform better than their traditional Gaussian counterparts [88]. Can this performance improvement be understood and generalized to more forms of generative modeling? Can non-equilibrium generative models such as diffusion models be accelerated using physical devices that harness natural sources of non-Gaussian noise?

More generally, our work hints at a new kind of computer: a computer that harnesses natural sources of non-Gaussian noise to accelerate probabilistic computations. The work presented in this thesis represents a starting point and a solid footing to stand on. We hope that we make significant further progress towards this goal in the coming years.

Bibliography

[1] C. E. Shannon, "A mathematical theory of communication," *The Bell system technical journal*, vol. 27, no. 3, pp. 379–423, 1948.

[2] C. Darwin, *On the origin of species by means of natural selection, or preservation of favoured races in the struggle for life.* London : John Murray, 1859. [Online]. Available: https://search.library.wisc.edu/catalog/9934839413602122

[3] T. McCourt, I. R. Fiete, and I. L. Chuang, "Noisy dynamical systems evolve error correcting codes and modularity," *arXiv preprint arXiv:2303.14448*, 2023.

[4] A. Eldar and M. B. Elowitz, "Functional roles for noise in genetic circuits," *Nature*, vol. 467, no. 7312, pp. 167–173, Sep 2010. [Online]. Available: https://doi.org/10.1038/nature09326

[5] R. Losick and C. Desplan, "Stochasticity and cell fate," *Science*, vol. 320, no. 5872, pp. 65–68, 2008. [Online]. Available: https://www.science.org/doi/abs/10.1126/science.1147888

[6] N. Q. Balaban, J. Merrin, R. Chait, L. Kowalik, and S. Leibler, "Bacterial persistence as a phenotypic switch," *Science*, vol. 305, no. 5690, pp. 1622–1625, 2004. [Online]. Available: https://www.science.org/doi/abs/10.1126/science.1099390

[7] G. Li, L.-K. Tam, and J. X. Tang, "Amplified effect of brownian motion in bacterial near-surface swimming," *Proceedings of the National Academy of Sciences*, vol. 105, no. 47, pp. 18 355–18 359, 2008. [Online]. Available: https://www.pnas.org/doi/abs/10.1073/pnas.0807305105

[8] J. Taktikos, H. Stark, and V. Zaburdaev, "How the motility pattern of bacteria affects their dispersal and chemotaxis," *PLOS ONE*, vol. 8, no. 12, pp. 1–8, 12 2014. [Online]. Available: https://doi.org/10.1371/journal.pone.0081936

[9] W. B. Whitman, D. C. Coleman, and W. J. Wiebe, "Prokaryotes: The unseen majority," *Proceedings of the National Academy of Sciences*, vol. 95, no. 12, pp. 6578–6583, 1998. [Online]. Available: https://www.pnas.org/doi/abs/10.1073/pnas.95.12.6578

[10] M. A. Wiering, "Explorations in efficient reinforcement learning," Ph.D. dissertation, Department of Mathematics and Computer Science, University of Amsterdam, 1999.

[11] A. Einstein, "On the motion of small particles suspended in a stationary liquid," *Ann. Phys*, vol. 322, no. 8, pp. 549–560, 1905.

[12] A. Simha, "Brownian motion in liquids: theory and experiment," Ph.D. dissertation, Department of Physics, The University of Texas at Austin, 2017.

[13] U. Vool and M. Devoret, "Introduction to quantum electromagnetic circuits," *International Journal of Circuit Theory and Applications*, vol. 45, no. 7, pp. 897–934, 2017. [Online]. Available: https://onlinelibrary.wiley.com/doi/abs/10.1002/cta.2359

[14] H. Mori, "Transport, Collective Motion, and Brownian Motion*)," *Progress of Theoretical Physics*, vol. 33, no. 3, pp. 423–455, 03 1965. [Online]. Available: https://doi.org/10.1143/PTP.33.423

[15] R. Kubo, "The fluctuation-dissipation theorem," *Reports on Progress in Physics*, vol. 29, no. 1, p. 255, jan 1966. [Online]. Available: https://dx.doi.org/10.1088/0034-4885/29/1/306

[16] H. C. Berg, *Random walks in biology*. Princeton University Press, 1993.

[17] J. Taktikos, H. Stark, and V. Zaburdaev, "How the motility pattern of bacteria affects their dispersal and chemotaxis," *PLOS ONE*, vol. 8, no. 12, pp. 1–8, 12 2014. [Online]. Available: https://doi.org/10.1371/journal.pone.0081936

[18] Y. Fily and M. C. Marchetti, "Athermal phase separation of self-propelled particles with no alignment," *Physical Review Letters*, vol. 108, 01 2012.

[19] E. Fodor, H. Hayakawa, J. Tailleur, and F. van Wijland, "Non-gaussian noise without memory in active matter," *Phys. Rev. E*, vol. 98, p. 062610, Dec 2018. [Online]. Available: https://link.aps.org/doi/10.1103/PhysRevE.98.062610

[20] S. Arrhenius, "On the heat of dissociation and the influence of temperature on the degree of dissociation of the electrolytes," *Zeitschrift für Physikalische Chemie (in German, Über die Dissociationswärme und den Einfluss der Temperatur auf den Dissociationsgrad der Elektrolyte)*, vol. 4, no. 1, pp. 96–116, 1889.

[21] A. Baule and P. Sollich, "Exponential increase of transition rates in metastable systems driven by non-gaussian noise," *Scientific Reports*, vol. 13, no. 1, p. 3853, Mar 2023. [Online]. Available: https://doi.org/10.1038/s41598-023-30577-0

[22] C. L. Degen, F. Reinhard, and P. Cappellaro, "Quantum sensing," *Rev. Mod. Phys.*, vol. 89, p. 035002, Jul 2017. [Online]. Available: https://link.aps.org/doi/10.1103/RevModPhys.89.035002

[23] P. Krantz, M. Kjaergaard, F. Yan, T. P. Orlando, S. Gustavsson, and W. D. Oliver, "A quantum engineer's guide to superconducting qubits," *Applied Physics Reviews*, vol. 6, no. 2, p. 021318, 06 2019. [Online]. Available: https://doi.org/10.1063/1.5089550

[24] J. Koch, T. M. Yu, J. Gambetta, A. A. Houck, D. I. Schuster, J. Majer, A. Blais, M. H. Devoret, S. M. Girvin, and R. J. Schoelkopf, "Charge-insensitive qubit design derived from the cooper pair box," *Physical Review A*, vol. 76, no. 4, Oct 2007. [Online]. Available: http://dx.doi.org/10.1103/PhysRevA.76.042319

[25] C. Neill, T. McCourt, X. Mi, Z. Jiang, M. Y. Niu, W. Mruczkiewicz, I. Aleiner, F. Arute, K. Arya, J. Atalaya, and et al., "Accurately computing the electronic properties of a quantum ring," *Nature*, vol. 594, no. 7864, p. 508–512, Jun 2021. [Online]. Available: http://dx.doi.org/10.1038/s41586-021-03576-2

[26] F. Arute, K. Arya, R. Babbush, D. Bacon, J. C. Bardin, R. Barends, A. Bengtsson, S. Boixo, M. Broughton, B. B. Buckley *et al.*, "Observation of separated dynamics of charge and spin in the fermi-hubbard model," *arXiv preprint arXiv:2010.07965*, 2020.

[27] A. T. Tan, S.-N. Sun, R. N. Tazhigulov, G. K.-L. Chan, and A. J. Minnich, "Realizing symmetry-protected topological phases in a spin-1/2 chain with next-nearest-neighbor hopping on superconducting qubits," *Physical Review A*, vol. 107, no. 3, p. 032614, 2023.

[28] F. Arute, K. Arya, R. Babbush, D. Bacon, J. C. Bardin, R. Barends, S. Boixo, M. Broughton, B. B. Buckley, and et al., "Hartree-fock on a superconducting qubit quantum computer," *Science*, vol. 369, no. 6507, p. 1084–1089, Aug 2020. [Online]. Available: http://dx.doi.org/10.1126/science.abb9811

[29] J. Kelly, R. Barends, A. G. Fowler, A. Megrant, E. Jeffrey, T. C. White, D. Sank, J. Y. Mutus, B. Campbell, Y. Chen, and et al., "State preservation by repetitive error detection in a superconducting quantum circuit," *Nature*, vol. 519, no. 7541, p. 66–69, Mar 2015. [Online]. Available: http://dx.doi.org/10.1038/nature14270

[30] Z. Chen, K. J. Satzinger, J. Atalaya, A. N. Korotkov, and et al., "Exponential suppression of bit or phase errors with cyclic error correction," *Nature*, vol. 595, no. 7867, pp. 383–387, Jul 2021. [Online]. Available: https://doi.org/10.1038/s41586-021-03588-y

[31] F. Arute *et al.*, "Quantum supremacy using a programmable superconducting processor," *Nature*, vol. 574, no. 7779, pp. 505–510, 2019. [Online]. Available: https://doi.org/10.1038/s41586-019-1666-5

[32] H.-Y. Huang, M. Broughton, J. Cotler, S. Chen, J. Li, M. Mohseni, H. Neven, R. Babbush, R. Kueng, J. Preskill *et al.*, "Quantum advantage in learning from experiments," *Science*, vol. 376, no. 6598, pp. 1182–1186, 2022.

[33] Y. Sung, L. Ding, J. Braumüller, A. Vepsäläinen, B. Kannan, M. Kjaergaard, A. Greene, G. O. Samach, C. McNally, D. Kim, A. Melville, B. M. Niedzielski, M. E. Schwartz, J. L. Yoder, T. P. Orlando, S. Gustavsson, and W. D. Oliver, "Realization of high-fidelity cz and zz-free iswap gates with a tunable

coupler," *Phys. Rev. X*, vol. 11, p. 021058, Jun 2021. [Online]. Available: https://link.aps.org/doi/10.1103/PhysRevX.11.021058

[34] B. Foxen, C. Neill, A. Dunsworth, P. Roushan, B. Chiaro, A. Megrant, J. Kelly, Z. Chen, K. Satzinger, R. Barends, and et al., "Demonstrating a continuous set of two-qubit gates for near-term quantum algorithms," *Physical Review Letters*, vol. 125, no. 12, Sep 2020. [Online]. Available: http://dx.doi.org/10.1103/PhysRevLett.125.120504

[35] G. S. Uhrig, "Exact results on dynamical decoupling by π pulses in quantum information processes," *New Journal of Physics*, vol. 10, 2008.

[36] L. Cywiński, R. M. Lutchyn, C. P. Nave, and S. Das Sarma, "How to enhance dephasing time in superconducting qubits," *Phys. Rev. B*, vol. 77, p. 174509, May 2008. [Online]. Available: https://link.aps.org/doi/10.1103/PhysRevB.77.174509

[37] J. Bylander, S. Gustavsson, F. Yan, F. Yoshihara, K. Harrabi, G. Fitch, D. G. Cory, Y. Nakamura, J. S. Tsai, and W. D. Oliver, "Noise spectroscopy through dynamical decoupling with a superconducting flux qubit," *Nature Physics*, vol. 7, no. 7, pp. 565–570, 2011.

[38] M. J. Biercuk, A. C. Doherty, and H. Uys, "Dynamical decoupling sequence construction as a filter-design problem," *Journal of Physics B: Atomic, Molecular and Optical Physics*, vol. 44, no. 15, 2011.

[39] X. You, A. A. Clerk, and J. Koch, "Positive- and negative-frequency noise from an ensemble of two-level fluctuators," *Phys. Rev. Research*, vol. 3, p. 013045, Jan 2021. [Online]. Available: https://link.aps.org/doi/10.1103/PhysRevResearch.3.013045

[40] L. M. Norris, G. A. Paz-Silva, and L. Viola, "Qubit noise spectroscopy for non-gaussian dephasing environments," *Phys. Rev. Lett.*, vol. 116, p. 150503, Apr 2016. [Online]. Available: https://link.aps.org/doi/10.1103/PhysRevLett.116.150503

[41] Y. Sung, F. Beaudoin, L. M. Norris, F. Yan, D. K. Kim, J. Y. Qiu, U. von Lüpke, J. L. Yoder, T. P. Orlando, S. Gustavsson, L. Viola, and W. D. Oliver, "Non-Gaussian noise spectroscopy with a superconducting qubit sensor," *Nature Communications*, vol. 10, no. 1, pp. 1–8, 2019. [Online]. Available: http://dx.doi.org/10.1038/s41467-019-11699-4

[42] G. A. Paz-Silva, L. M. Norris, and L. Viola, "Multiqubit spectroscopy of gaussian quantum noise," *Phys. Rev. A*, vol. 95, p. 022121, Feb 2017. [Online]. Available: https://link.aps.org/doi/10.1103/PhysRevA.95.022121

[43] P. Szańkowski, M. Trippenbach, and L. Cywiński, "Spectroscopy of cross correlations of environmental noises with two qubits," *Phys. Rev. A*, vol. 94, p. 012109, Jul 2016. [Online]. Available: https://link.aps.org/doi/10.1103/PhysRevA.94.012109

[44] J. Krzywda, P. Szankowski, and L. Cywinski, "The dynamical-decoupling-based spatiotemporal noise spectroscopy," *New Journal of Physics*, vol. 21, 03 2019.

[45] A. G. Kofman and A. N. Korotkov, "Two-qubit decoherence mechanisms revealed via quantum process tomography," *Phys. Rev. A*, vol. 80, p. 042103, Oct 2009. [Online]. Available: https://link.aps.org/doi/10.1103/PhysRevA.80.042103

[46] Y.-Q. Chen, K.-L. Ma, Y.-C. Zheng, J. Allcock, S. Zhang, and C.-Y. Hsieh, "Non-markovian noise characterization with the transfer tensor method," *Phys. Rev. Appl.*, vol. 13, p. 034045, Mar 2020. [Online]. Available: https://link.aps.org/doi/10.1103/PhysRevApplied.13.034045

[47] M. A. Rol, F. Battistel, F. K. Malinowski, C. C. Bultink, B. M. Tarasinski, R. Vollmer, N. Haider, N. Muthusubramanian, A. Bruno, B. M. Terhal, and L. DiCarlo, "Fast, high-fidelity conditional-phase gate exploiting leakage interference in weakly anharmonic superconducting qubits," *Phys. Rev. Lett.*, vol. 123, p. 120502, Sep 2019. [Online]. Available: https://link.aps.org/doi/10.1103/PhysRevLett.123.120502

[48] P. Dutta and P. M. Horn, "Low-frequency fluctuations in solids: $\frac{1}{f}$ noise," *Rev. Mod. Phys.*, vol. 53, pp. 497–516, Jul 1981. [Online]. Available: https://link.aps.org/doi/10.1103/RevModPhys.53.497

[49] R. J. Schoelkopf, P. Wahlgren, A. A. Kozhevnikov, P. Delsing, and D. E. Prober, "The radio-frequency single-electron transistor (RF-SET): A fast and ultrasensitive electrometer," *Science*, vol. 280, no. 5367, pp. 1238–1242, 1998.

[50] D. An, C. Matthiesen, E. Urban, and H. Häffner, "Distance scaling and polarization of electric-field noise in a surface ion trap," *Phys. Rev. A*, vol. 100, p. 063405, Dec 2019. [Online]. Available: https://link.aps.org/doi/10.1103/PhysRevA.100.063405

[51] F. Yoshihara, Y. Nakamura, F. Yan, S. Gustavsson, J. Bylander, W. D. Oliver, and J.-S. Tsai, "Flux qubit noise spectroscopy using rabi oscillations under strong driving conditions," *Phys. Rev. B*, vol. 89, p. 020503(R), Jan 2014. [Online]. Available: https://link.aps.org/doi/10.1103/PhysRevB.89.020503

[52] T. McCourt, C. Neill, K. Lee, C. Quintana, Y. Chen, J. Kelly, J. Marshall, V. N. Smelyanskiy, M. I. Dykman, A. Korotkov, I. L. Chuang, and A. G. Petukhov, "Learning noise via dynamical decoupling of entangled qubits," *Phys. Rev. A*, vol. 107, p. 052610, May 2023. [Online]. Available: https://link.aps.org/doi/10.1103/PhysRevA.107.052610

[53] F. Yan, P. Krantz, Y. Sung, M. Kjaergaard, D. L. Campbell, T. P. Orlando, S. Gustavsson, and W. D. Oliver, "Tunable Coupling Scheme for Implementing High-Fidelity Two-Qubit Gates," *Physical Review Applied*, vol. 10, no. 5, 2018.

[54] U. Vool and M. Devoret, "Introduction to quantum electromagnetic circuits," *International Journal of Circuit Theory and Applications*, vol. 45, no. 7, pp. 897–934, 2017. [Online]. Available: https://onlinelibrary.wiley.com/doi/abs/10.1002/cta.2359

[55] J. R. Schrieffer and P. A. Wolff, "Relation between the anderson and kondo hamiltonians," *Phys. Rev.*, vol. 149, pp. 491–492, Sep 1966. [Online]. Available: https://link.aps.org/doi/10.1103/PhysRev.149.491

[56] R. Koch, J. Clarke, W. Goubau, J. Martinis, C. Pegrum, and D. Van Harlingen, "Flicker (1/ f) noise in tunnel junction dc squids," *Low Temperature Physics - LOW TEMP PHYS*, vol. 51, pp. 207–224, 04 1983.

[57] P. Kumar, S. Sendelbach, M. A. Beck, J. W. Freeland, Z. Wang, H. Wang, C. C. Yu, R. Q. Wu, D. P. Pappas, and R. McDermott, "Origin and reduction of $1/f$ magnetic flux noise in superconducting devices," *Phys. Rev. Appl.*, vol. 6, p. 041001, Oct 2016. [Online]. Available: https://link.aps.org/doi/10.1103/PhysRevApplied.6.041001

[58] F. Yoshihara, K. Harrabi, A. O. Niskanen, Y. Nakamura, and J. S. Tsai, "Decoherence of flux qubits due to $1/f$ flux noise," *Phys. Rev. Lett.*, vol. 97, p. 167001, Oct 2006. [Online]. Available: https://link.aps.org/doi/10.1103/PhysRevLett.97.167001

[59] R. C. Bialczak, R. McDermott, M. Ansmann, M. Hofheinz, N. Katz, E. Lucero, M. Neeley, A. D. O'Connell, H. Wang, A. N. Cleland, and J. M. Martinis, "$1/f$ flux noise in josephson phase qubits," *Phys. Rev. Lett.*, vol. 99, p. 187006, Nov 2007. [Online]. Available: https://link.aps.org/doi/10.1103/PhysRevLett.99.187006

[60] J. Koch, T. M. Yu, J. Gambetta, A. A. Houck, D. I. Schuster, J. Majer, A. Blais, M. H. Devoret, S. M. Girvin, and R. J. Schoelkopf, "Charge-insensitive qubit design derived from the Cooper pair box," *Physical Review A - Atomic, Molecular, and Optical Physics*, vol. 76, no. 4, pp. 1–21, 2007.

[61] N. F. Ramsey, "A molecular beam resonance method with separated oscillating fields," *Phys. Rev.*, vol. 78, pp. 695–699, Jun 1950. [Online]. Available: https://link.aps.org/doi/10.1103/PhysRev.78.695

[62] H. Y. Carr and E. M. Purcell, "Effects of diffusion on free precession in nuclear magnetic resonance experiments," *Phys. Rev.*, vol. 94, pp. 630–638, May 1954. [Online]. Available: https://link.aps.org/doi/10.1103/PhysRev.94.630

[63] S. Meiboom and D. Gill, "Modified spin-echo method for measuring nuclear relaxation times," *Review of Scientific Instruments*, vol. 29, no. 8, pp. 688–691, 1958. [Online]. Available: https://doi.org/10.1063/1.1716296

[64] Y. Sung, F. Beaudoin, L. M. Norris, F. Yan, D. K. Kim, J. Y. Qiu, U. von Lüpke, J. L. Yoder, T. P. Orlando, S. Gustavsson, L. Viola, and W. D. Oliver, "Non-gaussian noise spectroscopy with a superconducting qubit sensor," *Nature Communications*, vol. 10, no. 1, sep 2019. [Online]. Available: https://doi.org/10.1038%2Fs41467-019-11699-4

[65] N. Ezzell, B. Pokharel, L. Tewala, G. Quiroz, and D. A. Lidar, "Dynamical decoupling for superconducting qubits: a performance survey," *arXiv preprint arXiv:2207.03670*, 2022.

[66] L. Viola, E. Knill, and S. Lloyd, "Dynamical decoupling of open quantum systems," *Phys. Rev. Lett.*, vol. 82, pp. 2417–2421, Mar 1999. [Online]. Available: https://link.aps.org/doi/10.1103/PhysRevLett.82.2417

[67] J. Bylander, S. Gustavsson, F. Yan, F. Yoshihara, K. Harrabi, G. Fitch, D. G. Cory, Y. Nakamura, J.-S. Tsai, and W. D. Oliver, "Noise spectroscopy through dynamical decoupling with a superconducting flux qubit," *Nature Physics*, vol. 7, no. 7, p. 565–570, May 2011. [Online]. Available: http://dx.doi.org/10.1038/nphys1994

[68] D. H. Slichter, R. Vijay, S. J. Weber, S. Boutin, M. Boissonneault, J. M. Gambetta, A. Blais, and I. Siddiqi, "Measurement-induced qubit state mixing in circuit qed from up-converted dephasing noise," *Physical Review Letters*, vol. 109, no. 15, Oct 2012. [Online]. Available: http://dx.doi.org/10.1103/PhysRevLett.109.153601

[69] F. Yan, S. Gustavsson, J. Bylander, X. Jin, F. Yoshihara, D. G. Cory, Y. Nakamura, T. P. Orlando, and W. D. Oliver, "Rotating-frame relaxation as a noise spectrum analyser of a superconducting qubit undergoing driven evolution." *Nature communications*, vol. 4, p. 2337, 2013.

[70] F. Yoshihara, Y. Nakamura, F. Yan, S. Gustavsson, J. Bylander, W. D. Oliver, and J.-S. Tsai, "Flux qubit noise spectroscopy using rabi oscillations under strong driving conditions," *Physical Review B*, vol. 89, no. 2, Jan 2014. [Online]. Available: http://dx.doi.org/10.1103/PhysRevB.89.020503

[71] E. Paladino, Y. M. Galperin, G. Falci, and B. L. Altshuler, "$1/f$ noise: Implications for solid-state quantum information," *Rev. Mod. Phys.*, vol. 86, pp. 361–418, Apr 2014. [Online]. Available: https://link.aps.org/doi/10.1103/RevModPhys.86.361

[72] P. Dutta and P. M. Horn, "Low-frequency fluctuations in solids: $\frac{1}{f}$ noise," *Rev. Mod. Phys.*, vol. 53, pp. 497–516, Jul 1981. [Online]. Available: https://link.aps.org/doi/10.1103/RevModPhys.53.497

[73] M. B. Weissman, "$\frac{1}{f}$ noise and other slow, nonexponential kinetics in condensed matter," *Rev. Mod. Phys.*, vol. 60, pp. 537–571, Apr 1988. [Online]. Available: https://link.aps.org/doi/10.1103/RevModPhys.60.537

[74] B. Savo, F. C. Wellstood, and J. Clarke, "Low-frequency excess noise in Nb-Al2O3-Nb Josephson tunnel junctions," *Applied Physics Letters*, vol. 50, no. 24, pp. 1757–1759, 06 1987. [Online]. Available: https://doi.org/10.1063/1.97738

[75] V. I. Klyatskin, *Lectures on Dynamics of Stochastic Systems*. Elsevier, Amsterdam, 2011.

[76] G. Ramon, "Non-gaussian signatures and collective effects in charge noise affecting a dynamically decoupled qubit," *Phys. Rev. B*, vol. 92, p. 155422, Oct 2015. [Online]. Available: https://link.aps.org/doi/10.1103/PhysRevB.92.155422

[77] Y. M. Galperin, B. L. Altshuler, J. Bergli, and D. V. Shantsev, "Non-gaussian low-frequency noise as a source of qubit decoherence," *Phys. Rev. Lett.*, vol. 96, p. 097009, Mar 2006. [Online]. Available: https://link.aps.org/doi/10.1103/PhysRevLett.96.097009

[78] L. Faoro and L. Viola, "Dynamical suppression of $1/f$ noise processes in qubit systems," *Phys. Rev. Lett.*, vol. 92, p. 117905, Mar 2004. [Online]. Available: https://link.aps.org/doi/10.1103/PhysRevLett.92.117905

[79] L. Cywiński, R. M. Lutchyn, C. P. Nave, and S. Das Sarma, "How to enhance dephasing time in superconducting qubits," *Phys. Rev. B*, vol. 77, p. 174509, May 2008. [Online]. Available: https://link.aps.org/doi/10.1103/PhysRevB.77.174509

[80] V. E. Shapiro and V. M. Loginov, ""Formulae of differentiation" and their use for solving stochastic equations," *Physica A: Statistical Mechanics and its Applications*, vol. 91, no. 3-4, pp. 563–574, 1978.

[81] J. Kelly, P. O'Malley, M. Neeley, H. Neven, and J. M. Martinis, "Physical qubit calibration on a directed acyclic graph," *arXiv preprint arXiv:1803.03226*, 2018.

[82] E. L. Hahn, "Spin echoes," *Phys. Rev.*, vol. 80, pp. 580–594, Nov 1950. [Online]. Available: https://link.aps.org/doi/10.1103/PhysRev.80.580

[83] D. Hayes, S. M. Clark, S. Debnath, D. Hucul, I. V. Inlek, K. W. Lee, Q. Quraishi, and C. Monroe, "Coherent error suppression in multiqubit entangling gates," *Phys. Rev. Lett.*, vol. 109, p. 020503, Jul 2012. [Online]. Available: https://link.aps.org/doi/10.1103/PhysRevLett.109.020503

[84] K. Mølmer and A. Sørensen, "Multiparticle entanglement of hot trapped ions," *Phys. Rev. Lett.*, vol. 82, pp. 1835–1838, Mar 1999. [Online]. Available: https://link.aps.org/doi/10.1103/PhysRevLett.82.1835

[85] Y. LeCun, S. Chopra, R. Hadsell, M. Ranzato, and F. Huang, "A tutorial on energy-based learning," *Predicting structured data*, vol. 1, no. 0, 2006.

[86] P. J. Rossky, J. D. Doll, and H. L. Friedman, "Brownian dynamics as smart monte carlo simulation," *The Journal of Chemical Physics*, vol. 69, no. 10, pp. 4628–4633, 1978.

[87] Y. Song, J. Sohl-Dickstein, D. P. Kingma, A. Kumar, S. Ermon, and B. Poole, "Score-based generative modeling through stochastic differential equations," *arXiv preprint arXiv:2011.13456*, 2020.

[88] E. Nachmani, R. S. Roman, and L. Wolf, "Non gaussian denoising diffusion models," *arXiv preprint arXiv:2106.07582*, 2021.